INFORMATION TO USERS

Rockets, magnetics and spin: A theoretical perspective

by

Michael V. Pak

A dissertation submitted to the graduate faculty

in partial fulfillment of the requirements for the degree of

DOCTOR OF PHILOSOPHY

Major: Physical Chemistry

Program of Study Committee:
Mark Gordon (Major Professor)
James W. Evans
Fritz H. Franzen
David K. Hoffman
Gordon J. Miller

Iowa State University

Ames, Iowa

2002

Graduate College
Iowa State University

This is to certify that the doctoral dissertation of

MICHAEL V. PAK

has met the dissertation requirements of Iowa State University

Signature was redacted for privacy.

Committee Member

Signature was redacted for privacy.

Committee Member

Signature was redacted for privacy.

Committee Member

Signature was redacted for privacy.

Committee Member

Signature was redacted for privacy.

Major Professor

Signature was redacted for privacy.

For the Major Program

To my parents

&

To Tanya

τα πολλα δε παλαι προκοψασ' - ου πονου πολλου με δει

μοχθειν δε βροτοισιν ανανκη....

TABLE OF CONTENTS

CHAPTER 1: GENERAL INTRODUCTION

I. Dissertation   Organization

Modern quantum chemistry as a science usually presents itself in two different aspects: the development of new theoretical methods and the application of existing methods to chemical problems. This Dissertation addresses both the theoretical and the applied side of quantum chemistry, and thus can be divided in two parts.

The first, theoretical, part includes Chapters 2 through 4 and deals with various theoretical problems of calculating magnetic properties of molecules, related to the electron spin density at the nuclei. Chapter 2 provides a review of mechanisms responsible for the indirect spin-spin coupling and contains a modified derivation of formulae for analytical calculation of spin-spin coupling constants at the restricted Hartree-Fock (RHF) level of theory, currently being implemented in the widely available quantum chemistry program GAMESS [1]. This Chapter also discusses possibilities for incorporating solvation effects into the calculation of spin-spin coupling.

Chapter 3 addresses various issues related to the calculation of electronic spin density at the nuclei, in particular the suitability of Gaussian basis sets for such calculations and the required level to account for electron correlation.

In Chapter 4, an analytic method for calculating the hyperfine coupling tensors for the second order multi-configurational quasidegenerate perturbation theory (MC QDPT) is derived within the response function formalism.

Chapters 5 and 6 constitute the second part of the dissertation and deal with application of various methods of quantum chemistry to the study

of the reaction of aluminum atoms with molecular oxygen. Chapter 5 is a study of the electronic structure of AlO_2 - an important intermediary in the Al combustion reaction. Chapter 6 presents a multi-configurational study of the potential energy surfaces for the $Al + O_2$ system.

Chapters 3 through 6 are papers either published, submitted to, or in preparation for submission to refereed journals. Chapter seven contains general conclusions for the entire Dissertation.

II. Magnetic Properties

Nuclear spin-spin coupling constants are among the most interesting and yet arguably the most difficult to calculate properties of a molecule. They depend on the chemical environment of the nuclei concerned and because of that contain a lot of information about the molecular electronic structure. These constants are also relatively easy to compare with experiment, since they can be obtained directly from NMR spectra and do not depend on the value of the applied field in an NMR experiment.

Chapter 2 contains a brief review of mechanisms responsible for the indirect spin-spin coupling, observed in high-resolution NMR experiments. The difficulty of calculating the spin-spin coupling by standard methods of quantum chemistry arises from the fact that in most cases the largest contribution to the nuclear spin-spin interactions is provided by the so called *contact* interaction between the electron and nuclear spins [2-3]. This type of interaction, also known as the Fermi contact interaction, is proportional (in the non-relativistic theory) to the electron spin density at the positions of the nuclei. The spin density at a given point in space is determined by the amplitude of the wave function at that point, and since most approximate molecular wave functions are optimized by some kind of global energy criterion, they may have significant errors at certain points in space. Indeed,

obtaining a wave function that very accurately describes some global properties of the molecule, - like transition energies or polarizabilities, does not guarantee that this wave function will behave correctly in a very small region around the nuclei.

Calculating the spin density at the nuclei presents even more difficult problems for standard quantum-chemical methods, since the majority of these methods employ Gaussian basis sets to approximate molecular orbitals. However, Gaussian functions have zero radial slope at the nucleus and are unable to satisfy the cusp condition associated with the singularity of the Coulomb potential at the nucleus. Chapter 3 deals with some of the problems associated with the suitability of Gaussian basis sets for spin density calculations, as well as with the required level of treatment of electron correlation.

Accurate evaluation of spin density at the nuclei and of the total indirect spin-spin coupling often requires a very high level of electron correlation treatment. There are a variety of standard correlated methods available for the calculation of spin-spin coupling constants, including the Moller-Plesset perturbation theory (MP), the coupled-cluster theory (CC) and various levels of configuration interaction (CI) treatment. However, all these methods are only applicable to systems that are well described by a single configuration. If static correlation is important, the description of the molecular electronic structure must be based on the multi-configurational SCF (MCSCF) wave function. However, the only multi-determinant method for which analytical calculation of spin-spin coupling is currently available is the MCSCF theory itself. In Chapter 4, a combined analytical-numerical method is proposed for calculating spin-spin coupling for MCQDPT theory. This method involves analytical calculation of hyperfine splitting tensors using the response function formalism.

III. Al as a HEDM additive to solid H_2

In the second part of this Dissertation, *ab-initio* methods of quantum chemistry are applied to the study of mechanisms of reactions of aluminum atoms with O_2. This study is motivated by the proposed use of atomic Al as a high energy density material (HEDM) additive to solid H_2. The expected improvement of energetic properties of solid molecular hydrogen used as a rocket propellant can be best understood in terms of the so called *specific impulse* (I_{SP}) of a rocket. By definition, the specific impulse is the amount of thrust achieved for the weight of fuel burned. However, it can also be thought of as a measure of the overall efficiency of a rocket engine. The specific impulse of a rocket propellant is a rough measure of how fast the propellant is ejected. The exhaust speed is primarily determined by the temperature of combustion and the molecular weight of the fuel. The following expression parametrizes the specific impulse as a function of the enthalpy of combustion of the fuel ΔH and the molecular mass of the exhaust gases M:

$$I_{SP} \sim \left(\frac{\Delta H}{M}\right)^{1/2} \tag{1}$$

As can be seen from Eq(1), the specific impulse of solid hydrogen used as a rocket fuel can be increased by additives with low molecular weight and high enthalpy of combustion. Depositing certain atomic species in solid hydrogen at just 5% concentrations can increase the specific impulse by more than 20%. In addition to the increase in specific impulse, HEDM additives have the potential to increase propellant density, allowing for more compact vehicles, and thus for a higher percentage of deliverable payload weight to vehicle weight.

Aluminum, with its high enthalpy of combustion and relatively low atomic mass, appears to be a very good candidate for the role of a HEDM additive. It has been predicted that solid H_2 doped with 5% aluminum atoms

would be 80% more dense than liquid H_2, and would therefore give a 10% specific impulse increase, corresponding to a 200% payload increase [4]. However, this prediction is based on the assumption that all of the aluminum present in the system is oxidized into Al_2O_3. In fact, using pure solid H_2 is preferable over Al-doped H_2, if any other Al oxides are generated in substantial quantities as final products of combustion, since the exothermicities of all other aluminum oxides are much smaller than that of Al_2O_3 [5]. Therefore, it is important to develop a quantitative understanding of the energetics of aluminum combustion. Chapter 5 deals with the electronic structure of AlO_2 which is expected to play a key role in the $Al + O_2$ reaction. Chapter 6 presents a general study of the $Al + O_2$ reaction, including the potential energy surfaces for the $Al + O_2$ system as well as possible mechanisms of the reactions of AlO with AlO_2 to form Al_2O_3.

IV. Theoretical Methods

This section contains a brief review of standard quantum chemical methods used throughout this Dissertation.

The simplest *ab initio* approach to solving the Shrödinger equation for a molecular system is the Hartree-Fock self-consistent field approximation (SCF). The molecular wave function is taken as an antisymmetrized product (Slater determinant) of molecular orbitals. Each molecular orbital is a product of some spatial function and either α or β eigenfunction of the spin operator. In the Restricted Hartree-Fock theory (RHF), the spatial parts of each α, β electron pair in the Slater determinant are required to be identical. For systems with unpaired electrons this requirement represents a serious restriction. Indeed, the exchange interaction only affects electrons of the same spin, and in a system where the number of α or β electrons are not

equal, an unrestricted optimization of the wave function would always result in different forms of α vs. β orbitals. If this restriction is removed and the spatial parts of α and β molecular orbitals are allowed to vary independently, the resulting wave function permits a considerably more accurate representation of the electron density in open shell systems. This type of SCF theory is called the unrestricted Hartree-Fock (UHF) method. In most cases, the UHF wave function is not an eigenfunction of the total spin operator. This means that it is not possible to obtain pure spin states from UHF theory.

The number of molecular orbitals that can be obtained by solving Hartree-Fock equations is equal to the number of functions in the basis set used to approximate these orbitals. Those molecular orbitals that are not included in the HF wave function are called virtual orbitals. For a given basis set, the best possible approximation for the exact solution of the Shrödinger equation can be obtained as a linear combination of all possible antisymmetrized poducts of N molecular orbitals, where N is the number of electrons in the molecule. Each of these antisymmetrized products (configurations) can be considered to be the result of an excitation of one or several electrons in the HF wave function from occupied to virtual orbitals. The coefficients C_K in the linear combination of all possible configurations $\Psi_{FCI} = \sum_K C_K \Psi_K$ are optimized variationally. The resulting full configuration interaction (FCI) wave function is the most accurate solution of the Shrödinger equation for the basis set used.

For reasonably large basis sets, FCI calculations are prohibitively expensive even for small molecules. There are a variety of approaches that aim at recovering most of the energy difference between FCI and HF at a much smaller cost. In various CI methods, only configurations accounting for excitations up to a certain level are included into the CI expansion. For example, in the Singles and Doubles CI (SD-CI) approximation, only the singly

and doubly excited (relative to HF) configurations are included. In the coupled cluster (CC) method, the excitations are organized in a very specific form by using the exponential excitation operator $|CC\rangle = \exp(\hat{T})|HF\rangle$ $\hat{T} = \hat{T}_1 + \hat{T}_2 + ...$, where $\hat{T}_1$ produces single excitations, $\hat{T}_2$ double excitations, and so on.

Another commonly used method of improving the Hartree-Fock energy is perturbation theory. In the most popular scheme, Moller-Plesset Perturbation Theory (MP PT), the perturbation is chosen as the difference between the exact Hamiltonian and the sum of one-electron Fock operators, forming the zeroth-order, unperturbed, Hamiltonian.

The single determinant Hartree-Fock approach does not always represent a reasonable zeroth-order approximation to the wave function. In systems involving degenerate or near-degenerate configurations, the HF description is not even qualitatively correct. The generalization of Hartree-Fock theory to systems that are not well described by a single configuration is the multi-configurational SCF (MCSCF) theory. The MCSCF wave function is a linear combination of two or more configurations, and both the molecular orbitals and the CI coefficients are optimized variationally. In the most popular type of MCSCF theory, the Complete Active Space SCF (CASSCF) [6-7] methods, the orbital space is partitioned into three subspaces - inactive, active and virtual. The inactive orbitals are doubly occupied in all configurations, and the virtual orbitals are always unoccupied. Distributing the active electrons in the active orbitals in all possible ways produces the set of CASSCF configurations.

The same hierarchy of methods can be based on the MCSCF wave function as the HF based methods described above. In the multi-configurational version of SD-CI theory called multy-reference CI (SD) (MRCI(SD)), configurations representing all single and double excitations

from all CASSCF configurations are included in the CI expansion. The multi-reference coupled cluster (MRCC) approach is significantly more difficult than the HF based CC method, and has not yet gained much popularity. There are many different ways to formulate the multi-reference perturbation theory using an MCSCF wave function as the zeroth-order unperturbed wave function. The multi-reference analog of MP perturbation theory used in this Dissertation is described in detail in Chapter 4.

References

1. M.W.Schmidt, K.K.Baldridge, J.A.Boatz, S.T.Elbert, M.S.Gordon, J.H.Jensen, S.Koseki, N.Matsunaga, K.A.Nguyen, S.J.Su, T.L.Windus, M.Dupuis, J.A.Montgomery, J.Comp.Chem. 14, 1347 (1993)

2. N.F.Ramsey, E.M.Purcell, Phys.Rev. 85,143 (1952)

3. N.F.Ramsey, Phys.Rev. 91,303 (1953)

4. J.A.Sheehy, Proc.HEDM Contr.Conf. 12 (2001)

5. M.W.Chase, C.A.Davies, J.R.Downey, D.Frurip, R.A.McDonald, A.N.Syverup, JANAF Thermochemical Tables, J.Phys.Chem. Ref.Data, 14 (Suppl. No 1) (1985)

6. B.O.Roos, P.R.Taylor, P.E.M.Siegbahn, Chem.Phys., 48, 157 (1980)

7. K.Ruedenberg, M.W.Schmidt, M.M.Gilbert and S.T.Ebert, Chem.Phys. 71, 41, 51, 65 (1982)

CHAPTER 2: SPIN-SPIN COUPLING CONSTANTS - SCF THEORY

I. Introduction

It is well known that the fine structure observed in high resolution NMR spectra is caused by the interaction between the magnetic moments of neighbouring nuclei. The largest part of this interaction is the direct dipole-dipole interaction of nuclear dipoles, responsible for very broad absorption lines in the NMR spectra of solids. However, in liquids the direct dipole-dipole interaction through space is averaged to zero by the rapid tumbling of the molecules. What is left is the much weaker indirect nuclear spin-spin coupling, resulting from the interaction of nuclear dipoles mediated by the surrounding electrons. This interaction determines the multiplet splitting of NMR absorption lines in liquids and is independent of the value of the applied magnetic field. Because the indirect coupling is transmitted through the electron subsytem, it is very sensitive to many aspects of molecular electronic structure.

The first theoretical interpretation for the mechanisms of indirect spin-spin coupling was provided by Ramsey and Purcell [1,2]. Since then, a variety of quantum chemical methods have been applied to calculating the spin-spin coupling constants, and at present they can be computed at various levels of theory with most of the commonly available electronic structure codes. An extensive review by Helgaker, Jaszunski and Ruud [3] discusses the most important *ab initio* methods for calculation of indirect spin-spin coupling as well as the availability of those methods in different widely used quantum chemistry programs.

Calculations of spin-spin coupling are usually carried out in the gas phase. However, the indirect coupling is of greater importance for NMR spectra in the liquid phase, and accounting for solvent effects presents a

major problem for theoretical study of magnetic properties. The most common approach to including solvent effects in calculation of spin-spin coupling is the supermolecule model, where some of the neighbouring solvent molecules are explicitly included in the calculation for the solute molecule. Because of the large size of the resulting system, most such calculations are restricted to the Hartree-Fock level [3]. Several recent theoretical studies also employed various continuum models of solvation, which describe the solvent by a surrounding dielectric medium [3-4]. There appears to be much need for using considerably more sophisticated methods for treating solvent effects on magnetic properties, which would match the increased accuracy of describing spin-spin coupling in the gas phase calculations. The Effective Fragment Potential (EFP) [5] method available in the quantum chemistry package GAMESS [6] is one such method, and coupling it with *ab initio* calculations of indirect spin-spin coupling would provide a valuable tool for studying solvation effects on molecular electronic structure.

In this chapter, a modified derivation of the formalism for analytic calculation of indirect spin-spin coupling constants at the Hartree-Fock level of theory is presented in the form in which it is being coded in the electronic structure code GAMESS. The evaluation of specific one-electron integrals of spin-spin coupling operators is also discussed, as well as the problems related to incorporating the EFP model in the spin-spin coupling calculations.

II. Spin-spin coupling constants - general theory

The main features of the NMR spectrum can be adequately described by the solutions of the energy equation for a simple effective Hamiltonian, which can be written as

$$H_{eff} = \sum_K \vec{B}(1 - \vec{\sigma}_K)\vec{M}_K + \frac{1}{2}\sum_{K \neq L} \vec{M}_K(\overline{D}_{KL} + \overline{K}_{KL})\vec{M}_L \qquad (1)$$

where the nuclear magnetic moments $\vec{M}_K$ are related to the nuclear spin operators $\vec{I}_K$ as $\vec{M}_K = \gamma_k \hbar \vec{I}_K$. The nuclear gyromagnetic ratios γ_k can also be expressed in terms of the nuclear g factors and the nuclear Bohr magnetons: $\gamma_k \hbar = g_K \mu_B^K$. The first term in Eq. (1) describes the interaction of the applied magnetic field $\vec{B}$ with the magnetic moment $\vec{M}_K$, and includes the nuclear magnetic shielding tensor σ_k. The second term accounts for the spin-spin interaction, described by the classical dipolar interaction tensor $\overline{D}_{KL}$ and the indirect spin-spin coupling tensors $\overline{K}_{KL}$. For rapidly rotating molecules in an isotropic medium, the direct spin-spin coupling constants $\overline{D}_{KL}$ vanish after the rotational averaging of the spin Hamiltonian, and the entire spin-spin coupling is described by the reduced indirect spin-spin coupling constants $K_{KL} = \frac{1}{3} Tr \overline{K}_{KL}$. The isotropic spin-spin coupling Hamiltonian is then

$$H_{SS}^{iso} = \frac{1}{2} \sum_{K \neq L} \vec{M}_K K_{KL} \vec{M}_L \qquad (2)$$

Note that in NMR experiments another form of spin-spin coupling constants is often used - the indirect spin-spin coupling tensors $\overline{J}_{KL} = h \frac{\gamma_K}{\pi} \frac{\gamma_L}{\pi} \overline{K}_{KL}$, which explicitly depend on the gyromagnetic ratios of the interacting nuclei.

In experimental work the values for the indirect spin-spin coupling constants are determined so that the spectrum of the effective Hamiltonian Eq. (1) coincides with the observed NMR spectrum. From the theoretical perspective, these constants are related to the derivatives of the molecular energy, obtainable from the electronic wave function. This relationship is best understood in the framework of perturbation theory. Indeed, the contribution to the total energy due to nuclear spin-spin interactions is very small, on the order of 10^{-13} a.u. [3], thus justifying the use of perturbation

approaches. Expand the electronic energy in the nuclear magnetic moments $\vec{M}_K$ around zero magnetic moments

$$E(\vec{M}) = E^{(0)} + \sum_K E_K^{(1)} \vec{M}_K + \frac{1}{2} \sum_{K \neq L} E_{KL}^{(2)} \vec{M}_K \vec{M}_L \tag{3}$$

Here $E_K^{(1)} = \left. \dfrac{dE(M)}{dM_K} \right|_{M=0}$ and $E_K^{(2)} = \left. \dfrac{d^2E(M)}{dM_K dM_L} \right|_{M=0}$, and the higher order terms

may be neglected due to the smallness of the perturbation. Comparing Eq.(3) with the effective Hamiltonian in Eq.(1), the second derivative of the energy $E_K^{(2)}$ can be identified with the spin-spin coupling

$$E_K^{(2)} = D_{KL} + K_{KL} \tag{4}$$

Thus, the spin-spin coupling constants can be calculated from second derivatives of the molecular energy with respect to the nuclear magnetic moments. In nondegenerate perturbation theory for a variational wave function, the first order expression for the second derivative of the electronic energy

$$\frac{d^2E(M)}{dM_K dM_L} = \left\langle \Psi_0 \left| \frac{d^2H}{dM_K dM_L} \right| \Psi_0 \right\rangle - 2 \sum_{n \neq 0} \frac{\left\langle \Psi_0 \left| \frac{dH}{dM_K} \right| \Psi_n \right\rangle \left\langle \Psi_n \left| \frac{dH}{dM_L} \right| \Psi_0 \right\rangle}{E_n - E_0} \tag{5}$$

includes two terms: the expectation value of the second derivative of the molecular Hamiltonian H for the unperturbed ground state wave function Ψ_0, and the sum of contributions from all excited states Ψ_n with energy E_n. For magnetic derivatives, the second term is commonly referred to as the paramagnetic part, and the expectation-value term is known as the diamagnetic part.

To obtain explicit expressions for the energy derivative, the first and the second order perturbation corrections to the Hamiltonian $\dfrac{dH}{dM_K}$ and

$\dfrac{d^2H}{dM_K dM_L}$ need to be derived. Consider the unperturbed molecular

Hamiltonian

$$\hat{H} = \frac{1}{2}\sum_i \vec{p}_i^2 - \sum_{iK}\frac{Z_K}{r_{iK}} + \frac{1}{2}\sum_{K \neq L}\frac{Z_K Z_L}{R_{KL}} + \frac{1}{2}\sum_{i \neq j}\frac{1}{r_{ij}} \tag{6}$$

The presence of nuclear magnetic moments results in several contributions to this standard Hamiltonian of molecular quantum mechanics. First, a term describing the direct interaction of the magnetic moments has to be introduced: $\sum_{K>L}\vec{M}_K D_{KL}\vec{M}_L$. Second, each magnetic moment $\vec{M}_K$ generates a

magnetic field with vector potential $\vec{A}_K(\vec{r}_i) = \alpha\dfrac{\vec{M}_K \times \vec{r}_{iK}}{r_{iK}^3}$ (where α is the fine

structure constant) and magnetic induction $\vec{B}_K(\vec{r}_i) = \vec{\nabla}_i \times \vec{A}_K(\vec{r}_i)$. The total magnetic field created by magnetic moments of all nuclei in the molecule is the sum of contributions from each nucleus:

$$\vec{A}(\vec{r}_i) = \sum_K \vec{A}_K(\vec{r}_i) \qquad\qquad \vec{B}(\vec{r}_i) = \sum_K \vec{B}_K(\vec{r}_i) \tag{7}$$

This magnetic field interacts with magnetic moments of electrons, contributing $-\sum_i \vec{m}_i \vec{B}(\vec{r}_i)$ to the Hamiltonian, and with magnetic moments of

nuclei, contributing $-\sum_K \vec{M}_K \vec{B}(\vec{r}_K)$. The magnetic moment of the electrons $\vec{m}_i$

is related to the electron spin operator as $\hat{m}_i = -\hat{s}_i$, assuming that the electron g factor is equal to 2 and the Bohr magneton is 1/2 in atomic units. Finally, in the presence of a magnetic field the momentum operators have to be replaced by so called 'generalized' momentum operators, accounting for the gage invariance of the electron field: $\vec{p}_i \rightarrow \vec{P}_i = \vec{p}_i + \vec{A}(\vec{r}_i) = -i\vec{\nabla}_i + \vec{A}(\vec{r}_i)$. The resulting molecular electronic Hamiltonian may be written in atomic units as

$$\hat{H}(\vec{M}) = \frac{1}{2}\sum_i \left[-i\vec{\nabla}_i + \vec{A}(\vec{r}_i)\right]^2 - \sum_{iK}\frac{Z_K}{r_{iK}} + \frac{1}{2}\sum_{K\ne L}\frac{Z_K Z_L}{R_{KL}} + \frac{1}{2}\sum_{i\ne j}\frac{1}{r_{ij}}$$
$$- \sum_i \vec{m}_i \vec{B}(\vec{r}_i) - \sum_K \vec{M}_K \vec{B}(\vec{r}_K) + \sum_{K>L}\vec{M}_K D_{KL}\vec{M}_L \tag{8}$$

To reveal the explicit dependence of the perturbed Hamiltonian Eq. (8) on the magnetic moments $\vec{M}_K$, the contributions to the magnetic induction

$\vec{B}_K(\vec{r}_i) = \alpha\left[\vec{\nabla}_i \times \dfrac{\vec{M}_K \times \vec{r}_{iK}}{r_{iK}^3}\right]$ need to be evaluated. The mathematical details of

calculating the curl of a singular vector field are presented in the Appendix. The resulting contribution to the total magnetic induction from the magnetic moment $\vec{M}_K$ is

$$\vec{B}_K(\vec{r}_i) = -\alpha^2\left[\frac{r_{iK}^2 - 3\vec{r}_{iK}\vec{r}_{iK}^T}{r_{iK}^5}\right]\vec{M}_K + \frac{8\pi\alpha^2}{3}\delta(\vec{r}_{iK})\vec{M}_K \tag{9}$$

where $\vec{r}_{iK}\vec{r}_{iK}^T$ is a second rank tensor formed from vector $\vec{r}_{iK}$ and transposed vector $\vec{r}_{iK}^T$.

The perturbations $\dfrac{dH}{dM_K}$ and $\dfrac{d^2H}{dM_K dM_L}$ can now be obtained by

differentiating the Hamiltonian Eq. (8) with respect to the nuclear magnetic moments $\vec{M}_K$. The first order correction is the hyperfine coupling operator $\hat{H}_K$, containing three distinct contributions:

$$\frac{dH}{dM_K} = \hat{H}_K^{(1)} = \hat{h}_K^{PSO} + \hat{h}_K^{SD} + \hat{h}_K^{FC} \tag{10}$$

These contributions are the paramagnetic spin-orbit (PSO) operator

$$\hat{h}_K^{PSO} = \alpha^2 \sum_i \frac{-\vec{r}_{iK} \times i\vec{\nabla}_i}{r_{iK}^3} \tag{11}$$

the spin-dipole (SD) operator

$$\hat{h}_K^{SD} = \alpha^2 \sum_i \frac{r_{iK}^2 \vec{m}_i - 3(\vec{m}_i \cdot \vec{r}_{iK})\vec{r}_{iK}}{r_{iK}^5} \tag{12}$$

and the Fermi contact (FC) operator

$$\hat{h}_K^{FC} = \frac{8\pi\alpha^2}{3} \sum_i \delta(r_{iK})\vec{m}_i \tag{13}$$

The PSO operator couples the nuclear magnetic moments to the orbital moments of the electrons (it is also known as the orbital hyperfine operator). The SD and FC operators couple the nuclear magnetic moments to the electron magnetic moments. In most systems, the FC interaction is the dominant mechanism of indirect spin-spin coupling.

The second order interaction term is obtained by differentiating the Hamiltonian Eq. (8) twice with respect to the magnetic moments $\vec{M}_K$ and $\vec{M}_L$ at zero magnetic moments:

$$\frac{d^2H}{dM_K dM_L} = \hat{H}_{KL}^{(2)} = D_{KL} + \hat{h}_{KL}^{DSO} \tag{14}$$

where $\hat{h}_{KL}^{DSO}$ is the diamagnetic electron operator

$$\hat{h}_{KL}^{DSO} = \frac{\alpha^2}{2} \sum_i \frac{(\vec{r}_{iK} \cdot \vec{r}_{iL}) - \vec{r}_{iK} \cdot \vec{r}_{iL}^T}{r_{iK}^3 r_{iL}^3} \tag{15}$$

Before proceeding to the calculation of energy derivatives for RHF theory, it is important to note the effect of the magnetic operators on a single determinant closed-shell wave function. From the form of the operators in Eqs.(11-13) it follows that $\hat{h}_K^{PSO} |RHF>$ is an imaginary singlet, while $\hat{h}_K^{SD} |RHF>$ and $\hat{h}_K^{FC} |RHF>$ are real triplet wave functions. The triplet character of the SD and FC operators is due to the presence of the electron spin operator $\hat{s}_i$, related to the electron magnetic moment $\hat{m}_i = -\hat{s}_i$. As a result, these operators act differently on α and β orbitals, creating a triplet contribution to the wave function. Thus, the first order magnetic

perturbation transforms a closed-shell HF wave function into a combination of imaginary singlet and real triplet wave functions. As a result, an RHF wave function is often not flexible enough to properly accommodate the effects of operators responsible for indirect spin-spin coupling. This problem is discussed further in chapter 4.

III. Evaluation of one-electron integrals

It follows from Eqs. (11-13) and Eq.(15) that calculation of spin-spin coupling constants at any level of theory will require evaluation of four types of integrals with Gaussian functions. These are the PSO integrals

$$\left\langle \Phi(\vec{r}_{iI} \mid n_I, l_I, m_I, \alpha_I) \left| \frac{-\vec{r}_{iK} \times i\vec{\nabla}_i}{r_{iK}^3} \right| \Phi(\vec{r}_{iJ} \mid n_J, l_J, m_J, \alpha_J) \right\rangle, \quad \text{the} \quad \text{SD} \quad \text{integrals}$$

$$\left\langle \Phi(\vec{r}_{iI} \mid n_I, l_I, m_I, \alpha_I) \left| \frac{r_{iK}^2 \vec{m}_i - 3(\vec{m}_i \cdot \vec{r}_{iK})\vec{r}_{iK}}{r_{iK}^5} \right| \Phi(\vec{r}_{iJ} \mid n_J, l_J, m_J, \alpha_J) \right\rangle \quad \text{the FC integrals}$$

$$\left\langle \Phi(\vec{r}_{iI} \mid n_I, l_I, m_I, \alpha_I) \left| \delta(\vec{r}_{iK})\vec{m}_i \right| \Phi(\vec{r}_{iJ} \mid n_J, l_J, m_J, \alpha_J) \right\rangle \quad \text{and} \quad \text{the} \quad \text{DSO} \quad \text{integrals}$$

$$\left\langle \Phi(\vec{r}_{iI} \mid n_I, l_I, m_I, \alpha_I) \left| \frac{(\vec{r}_{iK} \cdot \vec{r}_{iL}) - \vec{r}_{iK} \cdot \vec{r}_{iL}^T}{r_{iK}^3 r_{iL}^3} \right| \Phi(\vec{r}_{iJ} \mid n_J, l_J, m_J, \alpha_J) \right\rangle. \quad \text{Here}$$

$\Phi(\vec{r}_{iK} \mid n_K, l_K, m_K, \alpha_K)$ is the standard Cartesian Gaussian function

$$\Phi(\vec{r}_{iK} \mid n_K, l_K, m_K, \alpha_K) = x_{iK}^{n_K} y_{iK}^{l_K} z_{iK}^{m_K} \exp(-\alpha_K r_{iK}^2) \qquad (16)$$

centered at the nucleus K, and its angular momentum is given by the prefactor. For example, an s-function has $(n_I + l_I + m_I) = 0$, for a d-function $(n_I + l_I + m_I) = 2$, etc.

The calculation of FC integrals is trivial, involving only the evaluation of Gaussian functions centered on nuclei I and J at the position of nucleus K. The PSO integrals are evaluated using the Rys polynomials method [7] including a small modification of the scheme for calculating spin-orbit integrals, already implemented in GAMESS by Furlani [8].

For evaluation of SD integrals, the method suggested by Vahtras et al. [9] is currently being implemented. The integrals are calculated in terms of field-gradient integrals using the McMurchie-Davidson scheme [10]. The field-gradient integrals contain both SD and FC contributions [9]

$$\vec{\nabla} \times \frac{\vec{m} \times \vec{r}}{r^3} = \left(\frac{3\vec{r}\vec{r}^T - r^2}{r^5} + \frac{8\pi}{3}\delta(\vec{r}) \right)\vec{m} \tag{17}$$

Therefore, the previously computed FC integrals have to be subtracted from the calculated field-gradient integrals to obtain the SD integrals.

Evaluation of DSO integrals has been implemented in two different schemes. In a numerical method proposed by Matsuoka et al. [11], the second part of the DSO operator $\dfrac{\vec{r}_{iK} \cdot \vec{r}_{iL}^T}{r_{iK}^3 r_{iL}^3}$ is transformed using the following relation:

$$\frac{x_{iK}}{r_{iK}^3} = \frac{4}{\sqrt{\pi}} \int_0^\infty d\alpha_K \cdot \alpha_K^2 \cdot x_{iK} \exp(-\alpha_K r_{iK}^2) = \frac{4}{\sqrt{\pi}} \int_0^\infty d\alpha_K \cdot \alpha_K^2 \cdot \Phi(r_{iK} \mid 1,0,0,\alpha) \tag{18}$$

which can be applied to any components of $\dfrac{\vec{r}_{iK}}{r_{iK}^3}$. For example, a similar

transformation of the operator $\dfrac{z_{iK}}{r_{iK}^3}$ results in an integral involving the p_z-type

Gaussian function $\Phi(\vec{r}_{iK} \mid 0,0,1,\alpha)$. Applying this transformation to all

components of both $\dfrac{\vec{r}_{iK}}{r_{iK}^3}$ and $\dfrac{\vec{r}_{iL}}{r_{iL}^3}$, the DSO integrals can be reduced to

$$\left\langle \Phi_I \left| \frac{x_{iK}}{r_{iK}^3} \frac{x_{iL}}{r_{iL}^3} \right| \Phi_J \right\rangle = \frac{16}{\pi} \int_0^\infty \int_0^\infty d\alpha \cdot \alpha_K^2 \cdot d\alpha_L \cdot \alpha_J^2 < \Phi_I \Phi_K \Phi_L \Phi_J > \tag{19}$$

where $< \Phi_I \Phi_K \Phi_L \Phi_J >$ is a four-center overlap integral of four Gaussian functions, of which the middle two Gaussians are always of p-type. These four-center exchange intagrals are already available in the grid-free DFT

package in GAMESS. The integrals Eq. (19) are computed numerically, using the Gauss-Legendre quadrature [11].

However, the numerical integration approach, at least in our implementation, appears to be much slower than the direct evaluation of the DSO integrals using the resolution of the identity [12]. Using the converged HF molecular orbitals Ψ_v to expand the identity operator $\hat{E} = \sum_v |\Psi_v \rangle \langle \Psi_v|$, components of the DSO operator can be written as

$$\left\langle \Phi_I \left| \frac{x_{iK}}{r_{iK}^3} \frac{x_{iL}}{r_{iL}^3} \right| \Phi_J \right\rangle = \sum_v \left\langle \Phi_I \left| \frac{x_{iK}}{r_{iK}^3} \right| \Psi_v \right\rangle \left\langle \Psi_v \left| \frac{x_{iL}}{r_{iL}^3} \right| \Phi_J \right\rangle \tag{20}$$

Since every Ψ_v is a linear combination of atomic Gaussian orbitals, the products $\left\langle \Phi_I \left| \frac{x_{iK}}{r_{iK}^3} \right| \Psi_v \right\rangle \left\langle \Psi_v \left| \frac{x_{iL}}{r_{iL}^3} \right| \Phi_J \right\rangle$ in Eq. (20) can be expressed in terms of

integrals of Gaussian functions $\left\langle \Phi_I \left| \frac{x_{iK}}{r_{iK}^3} \right| \Phi_A \right\rangle \left\langle \Phi_B \left| \frac{x_{iL}}{r_{iL}^3} \right| \Phi_J \right\rangle$, where the integrals

$\left\langle \Phi_v \left| \frac{x_{iL}}{r_{iL}^3} \right| \Phi_J \right\rangle$, required in calculations of molecular polarizabilities, are

available in GAMESS. The number of molecular orbitals Ψ_v to be used in the expansion Eq. (20) is determined by comparing with the results of numerical integration. In principle, an expansion $\sum_v |\Psi_v \rangle \langle \Psi_v|$ is exactly equal to the identity operator only if the summation runs over a complete set of functions $\{\Psi_v\}$. However, reasonable accuracy can be achieved with smaller sets of basis functions, although this brings in a certain dependence of the results on the number of functions used in the expansion.

IV. RHF spin-spin   coupling   constants

As was mentioned above, the first order magnetic perturbations
transform the RHF wave function into a combination of imaginary singlet and
real triplet wave functions. Such transformations are more convenient to deal
with using the formalism of second quantization, in which both the wave
function and the perturbation operator are described uniformly in terms of
singlet and triplet excitation operators. Using creation operators $\hat{a}^+_{p\alpha}$, $\hat{a}^+_{p\beta}$ and
annihilation operators $\hat{a}_{p\alpha}$, $\hat{a}_{p\beta}$ associated with molecular spin-orbitals $\Psi_{p\alpha}$,
$\Psi_{p\beta}$, we define the unitary group generators $\hat{E}_{pq} = \hat{a}^+_{p\alpha}\hat{a}_{q\alpha} + \hat{a}^+_{p\beta}\hat{a}_{q\beta}$, which can
also be interpreted as singlet excitation operators. The triplet excitation
operators $\hat{T}_{pq} = \{\hat{T}^x_{pq}, \hat{T}^y_{pq}, \hat{T}^z_{pq}\}$ in Cartesian form can be written as

$$\hat{T}^x_{pq} = \frac{1}{2}\left(\hat{a}^+_{p\alpha}\hat{a}_{q\beta} + \hat{a}^+_{p\beta}\hat{a}_{q\alpha}\right)$$
$$\hat{T}^y_{pq} = \frac{1}{2i}\left(\hat{a}^+_{p\alpha}\hat{a}_{q\beta} - \hat{a}^+_{p\beta}\hat{a}_{q\alpha}\right) \qquad (21)$$
$$\hat{T}^z_{pq} = \frac{1}{2}\left(\hat{a}^+_{p\alpha}\hat{a}_{q\alpha} - \hat{a}^+_{p\beta}\hat{a}_{q\beta}\right)$$

Using the excitation operators $\hat{E}_{pq}$ and $\hat{T}_{pq}$, the real and imaginary orbital
rotation operators can now be defined [13]:

$$\hat{E}^\pm_{pq} = \hat{E}_{pq} \pm \hat{E}_{qp}, \qquad \hat{T}^{\gamma\pm}_{pq} = \hat{T}^\gamma_{pq} \pm \hat{T}^\gamma_{qp} \qquad (22)$$

Here the operators $\hat{E}^-_{pq}$ and $\hat{T}^{\gamma+}_{pq}$ carry out real singlet and triplet rotations (γ
in the definition of triplet operators runs over the three Cartesian directions),
while the operators $i\hat{E}^+_{pq}$ and $i\hat{T}^{\gamma-}_{pq}$ are responsible for imaginary orbital
rotations between molecular orbitals p and q. A completely general form of
the orbital rotation operator [3] can now be written as

$$\hat{K} = i\sum_{p>q} {}^I k^s_{pq}\hat{E}^+_{pq} + \sum_{p>q} {}^R k^s_{pq}\hat{E}^-_{pq} + i\sum_\gamma\sum_{p>q} {}^I k^\gamma_{pq}\hat{T}^{\gamma-}_{pq} + \sum_\gamma\sum_{p>q} {}^R k^\gamma_{pq}\hat{T}^{\gamma+}_{pq} \qquad (23)$$

This operator is characterized by a set of parameters $\left\{{}^I k^s_{pq}, {}^R k^s_{pq}, {}^I k^\gamma_{pq}, {}^R k^\gamma_{pq}\right\}$ that
describe all possible rotations in the orbital space. Parameters ${}^R k^s_{pq}$ and ${}^I k^s_{pq}$

describe the real and imaginary singlet rotations respectively, while the parameters $^R k_{pq}^\gamma$ and $^I k_{pq}^\gamma$ describe the real and imaginary triplet rotations.

In standard HF theory, the RHF wave function is optimized by singlet real orbital rotations only, and therefore the general parametrizarion for this type of wave function can be written as

$$| RHF(\hat{K}^{(0)}) \rangle = \exp(-\sum_{p>q} {}^R k_{pq}^s \hat{E}_{pq}^-) | \Omega \rangle \tag{24}$$

where $\hat{K}^{(0)} = \sum_{p>q} {}^R k_{pq}^s \hat{E}_{pq}^-$ is the HF orbital rotation operator, and $|\Omega\rangle$ is some single-determinant trial function. The choice of initial orbitals in the trial function $|\Omega\rangle$ is relatively arbitrary. One possible choice is to use the atomic basis functions, although this choice may result in slower convergence of the HF optimization. The parameters $^R k_{pq}^s$ are found from variational optimization of RHF energy

$$E_{HF} = \langle RHF(\hat{K}^{(0)}) | \hat{H}_{HF} | RHF(\hat{K}^{(0)}) \rangle \tag{25}$$

However, when the magnetic perturbation operators are introduced in the Hamiltonian, the full set of rotations must be present in the wave function perturbation $\exp(-\hat{K}^{(1)}) | RHF \rangle$.

The first order magnetic perturbations $\hat{H}_K^{(1)}$ (Eq. (10)) in second quantization formalism is expressed in terms of second-quantized PSO, SD and FC operators:

$$\hat{h}_K^{PSO} = -i\alpha^2 \sum_{pq} \left\langle \Psi_p(\vec{r}_i) \left| \frac{\vec{r}_{iK} \times i\vec{\nabla}_i}{r_{iK}^3} \right| \Psi_q(\vec{r}_i) \right\rangle \hat{E}_{pq}^+$$

$$\hat{h}_K^{SD} = -\alpha^2 \sum_{pq} \left\langle \Psi_p(\vec{r}_i) \left| \frac{r_{iK}^2 - 3\vec{r}_{iK}\vec{r}_{iK}^T}{r_{iK}^5} \right| \Psi_q(\vec{r}_i) \right\rangle \hat{T}_{pq}^+ \tag{26}$$

$$\hat{h}_K^{FC} = \frac{8\pi\alpha^2}{3} \sum_{pq} \left\langle \Psi_p(\vec{r}_i) \left| \delta(\vec{r}_{iK}) \right| \Psi_q(\vec{r}_i) \right\rangle \hat{T}_{pq}^+$$

Finally, the second order perturbation $H_{KL}^{(2)}$, defined in Eq. (14), in second quantization is written as

$$\hat{H}_{KL}^{(2)} = D_{KL} + \hat{h}_K^{DSO} = D_{KL} + \frac{\alpha^2}{2}\sum_{pq}\left\langle\Psi_p(\vec{r}_i)\left|\frac{(\vec{r}_{iK}\cdot\vec{r}_{iL}) - \vec{r}_{iK}\cdot\vec{r}_{iL}^T}{r_{iK}^3 r_{iL}^3}\right|\Psi_q(\vec{r}_i)\right\rangle\hat{E}_{pq} \quad (27)$$

Having defined the unperturbed HF wave function and the perturbation operators, it is possible now to formulate the analytic expressions for the energy derivatives. The standard perturbation expansion of the HF energy [3,14] to second order is

$$E^{(0)} = <HF|\hat{H}_{HF}|HF>$$
$$E_K^{(1)} = <HF|\hat{H}_K^{(1)}|HF>$$
$$E_{KL}^{(2)} = <HF|\hat{H}_{KL}^{(2)}|HF> + <HF|\left[\hat{K}_L^{(1)},\hat{H}_K^{(1)}\right]|HF> \quad (28)$$

where the second derivative of the energy $E_K^{(2)}$ has previously been identified with the spin-spin coupling constant (Eq. (4)). The operator $\hat{K}_L^{(1)}$ describes the first order correction to the HF wave function: $\hat{K}_L^{(1)} = \dfrac{d\hat{K}^{(0)}}{d\vec{M}_L}$.

Of the set of parameters $\left\{{}^I k_{pq}^s,{}^R k_{pq}^s,{}^I k_{pq}^\gamma,{}^R k_{pq}^\gamma\right\}$ characterizing the optimized HF wave function, only the subset of real singlet orbital rotation parameters $\{{}^R k_{pq}^s\}$ is nonzero: $\hat{K}^{(0)} = \displaystyle\sum_{p>q}{}^R k_{pq}^s\hat{E}_{pq}^-$. However, due to the specific nature of the magnetic perturbations, the first order perturbation correction to the HF wave function $\hat{K}_L^{(1)}$ must include imaginary singlet and real triplet orbital rotations. The general form of the orbital rotation operator describing the perturbation to the RHF function due to the presence of nuclear magnetic moments is

$$\hat{K}_K^{(1)} = i\sum_{p>q}\frac{d^I k_{pq}^s}{d\vec{M}_K}\hat{E}_{pq}^+ + \sum_{p>q}\frac{d^R k_{pq}^s}{d\vec{M}_K}\hat{E}_{pq}^- + \sum_\gamma\sum_{p>q}\frac{d^R k_{pq}^\gamma}{d\vec{M}_K}\hat{T}_{pq}^{\gamma+} \quad (29)$$

In other words, even though all $\left\{{}^{I}k_{pq}^{s}, {}^{R}k_{pq}^{\gamma}\right\}$ are equal to zero (after the HF optimization), some of them may have non-zero derivatives with respect to nuclear magnetic moments.

The Hartree-Fock conditions in the zeroth and first order in perturbation theory can be written as [3]

$$< HF\left[\hat{K}^{(0)}, \hat{H}_{HF}\right]\middle| HF >= 0$$

$$< HF\left[\hat{K}_i^{(0)}, \hat{H}^{(1)}\right]\middle| HF >= -\sum_j < HF\left[\hat{K}_i^{(0)}, \left[\hat{K}_j^{(0)}, \hat{H}_{HF}\right]\right]\middle| HF > \hat{K}_j^{(1)} \quad (30)$$

The summation in the second equation above runs over all orbital rotations $j=pq$. The zeroth-order condition for the unperturbed RHF wave function is also known as the Brillouin theorem. The first-order conditions (second equation) represent a set of linear equations for the first order perturbation correction to the wave function. They can also be interpreted as the first-order response equations, discussed in chapter 4.

Combining Eq. (4) with Eq. (28) for the second derivative of the HF energy, as well as with equations for the first and second order magnetic perturbations to the Hamiltonian Eqs. (26,27), we obtain the final expression for the indirect spin-spin coupling constants K_{KL} for RHF theory:

$$K_{KL} =< HF \mid \hat{h}_{KL}^{DSO} \mid HF > + \sum_{p>q} < HF\left[i\hat{E}_{pq}^{+}, \hat{h}_{K}^{PSO}\right]\middle| HF > \frac{d^{I}k_{pq}^{s}}{d\vec{M}_{L}}$$

$$+ \sum_{\gamma}\sum_{p>q} < HF\left[\hat{T}_{pq}^{\gamma-}, \hat{h}_{K}^{SD} + \hat{h}_{K}^{FC}\right]\middle| HF > \frac{d^{R}k_{pq}^{\gamma}}{d\vec{M}_{L}} \quad (31)$$

Here we have taken into account that $< HF\left[\hat{K}_L^{(1)}, \hat{H}_K^{(1)}\right]\middle| HF >$ is nonzero only in two instances: when $\hat{H}_K^{(1)} = \hat{h}_K^{PSO}$ and $\hat{K}_L^{(1)} = i\sum_{p>q}\frac{d^{I}k_{pq}^{s}}{d\vec{M}_{L}}\hat{E}_{pq}^{+}$, or when

$\hat{H}_K^{(1)} = \hat{h}_K^{SD} + \hat{h}_K^{FC}$ and $\hat{K}_L^{(1)} = \sum_{\gamma}\sum_{p>q}\frac{d^{R}k_{pq}^{\gamma}}{d\vec{M}_{L}}\hat{T}_{pq}^{\gamma+}$. The perturbation correction $\hat{K}_L^{(1)}$ is

determined from the first order conditions Eq. (30), which can now be written as:

$$\sum_{r>s} < HF\left[i\hat{E}_{pq}^+,\left[i\hat{E}_{rs}^+,\hat{H}_{HF}\right]\right]HF > \frac{d'k_{rs}^s}{d\bar{M}_K} = - < HF\left[\left[i\hat{E}_{pq}^+,\hat{h}_K^{PSO}\right]HF >\right.$$

$$\sum_{r>s} < HF\left[\hat{T}_{pq}^{\gamma+},\left[\hat{T}_{rs}^{\gamma+},\hat{H}_{HF}\right]\right]HF > \frac{d^Rk_{pq}^\gamma}{d\bar{M}_K} = - < HF\left[\hat{T}_{pq}^{\gamma+},\hat{h}_K^{SD}+\hat{h}_K^{FC}\right]HF > \quad (32)$$

Eqs. (31,32) comprise the complete set of equations necessary for the analytic evaluation of the indirect coupling constants. The response equations Eq. (32) are solved iteratively, starting from some non-zero trial vector

$\left\{\dfrac{d'k_{pq}^s}{d\bar{M}_K},\dfrac{d^Rk_{pq}^\gamma}{d\bar{M}_K}\right\}$. In the current implementation in GAMESS, convergence for

the triplet equations is very poor. This can be attributed to the fact that only six out of the nine triplet equations are linearly independent [3]. A linear transformation of the triplet perturbation vector can be used to resolve this problem. Once the perturbation corrections to the wave function are calculated, computing the spin-spin coupling constants using Eq. (31) presents a relatively simple task.

V. Solvent effects

To understand various aspects of incorporating solvation effects into calculation of magnetic properties, it is convinent to classify these effects as direct or indirect [3]. The direct effects result from the polarization of the electronic structure of the solute molecule by the surrounding solvent molecules. The indirect effects arise from changes in molecular geometry caused by the surrounding medium.

Accounting for the indirect effects does not require any substantial modifications in the way magnetic properties are calculated. The changes in the molecular geometry caused by the solvent are described by the solvation

model used, and the spin-spin coupling constants computed at this new geometry fully incorporate the indirect solvent effects on the spin-spin interaction. There are some indications that for systems where the indirect spin-spin coupling constant is dominated by the Fermi contact contribution, the indirect effects are significantly more important than the direct effects caused by solvent molecules [15].

Accounting for the direct effects presents a more complex problem. It follows from the form of the indirect spin-spin coupling constants in RHF theory Eq. (31), that the solvent polarization effects can affect these constants through two different channels. First, the matrix elements of the perturbation operators (e.g., $<HF\,|\,\hat{h}_{KL}^{DSO}\,|\,HF>$, $<HF\,\big|[\,i\hat{E}_{pq}^{+},\hat{h}_{K}^{PSO}\,]\big|\,HF>$, etc.) should be calculated with a wave function reflecting the polarization effects caused by the solvent molecules. This part of the direct effects is accounted for by the EFP model through the polarizability term [5]. The wave function modified by the solvent molecules in the EFP method is then used to compute the spin-spin coupling, thus transferring some of the polarization effects to the coupling constants. Second, the polarization of the wave function of the solute by the solvent molecules also affects the perturbation correction to the orbital rotation operator $K^{(1)}$ (with components $\dfrac{d^{1}k_{pq}^{s}}{d\tilde{M}_{L}}$ in Eq. (31)). This operator is determined by the response equations Eq. (32). From these equations, it appears that the polarization effects are again limited to the changes in the zeroth-order HF wave function. It is therefore reasonable to expect that the bulk of the polarization effects on the spin-spin coupling will be accounted for if the unperturbed (by magnetic moments of the nuclei) HF wave function is calculated within the EFP model, and then used to calculate the coupling constants in the usual fashion.

VI. Conclusions

This chapter presents a revised formalism for analytic evaluation of indirect spin-spin coupling constants for RHF theory, in the form in which it is being implemented in the electronic structure code GAMESS. Our ultimate goal is to take advantage of the relatively sophisticated EFP method for treating solvent effects, already available in GAMESS, to analyze and understand how the surrounding solvent molecules affect the indirect spin-spin interactions. A considerable part of the solvent effects: the indirect effects due to changes in molecular geometry and the direct effects of polarization of the electronic structure caused by the solvent, can be included in the indirect spin-spin coupling calculations by using the HF wave function obtained from the EFP model to calculate the coupling constants.

References

1. N.Ramsey, E.Purcell, Phys.Rev. **85**, 143 (1952)

2. N.Ramsey, Phys.Rev. **91**, 303 (1953)

3. T.Helgaker, M.Jaszunski, K.Ruud, Chem. Rev. **99**, 293 (1999)

4. P.-O.Astrand, K.Mikkelsen, P.Jorgensen, K.Ruud, T.Helgaker, J.Chem.Phys. **108**, 2528 (1998)

5. W.Chen, M.S.Gordon, J.Chem.Phys. **105**, 11081 (1996)

6. M. W. Schmidt, K. K. Baldridge, J. A. Boatz, S. T. Elbert, M. S. Gordon, J. H. Jensen, S. Koseki, N. Matsunaga, K. A. Nguyen, S. J. Su, T. L. Windus, M. Dupuis, J. A. Montgomery, J.Comp.Chem. **14**, 1347 (1993)

7. H.F.King, M. Dupuis, J.Comp.Phys. **21**, 144 (1976)

8. T.Furlani, PhD Thesis (SUNY at Buffalo, 1984)

9. O.Vahtras, H.Ågren, P.Jørgensen, H.J.Jensen, S.Padkjær, T.Helgaker, J.Chem.Phys. **96**, 6120 (1992)

10. L.E.McMurchie, E.R.Davidson, J.Comp.Phys. **26**, 218 (1978)

11. D.Matsuoka, T.Aoyama, J.Chem.Phys. **73**, 5718 (1980)

12. O.Vahtras, J.Almlöf, M.W.Feyereisen, Chem.Phys.Lett. **213**, 514 (1993)

13. P.Jørgensen, J.Simons, *Second Quantization-Based Methods in Quantum Quemistry;* Academic Press: New York, 1981

14. J.Olsen, In *Lecture Notes in Quantum Chemistry*; B.O.Roos, Ed.; Springer-Verlag: Berlin, 1992, p 59

15. D.Chipman, private communication

CHAPTER 3: FULL CONFIGURATION INTERACTION AND MULTI-CONFIGURATIONAL SPIN DENSITY IN BORON AND CARBON ATOMS

Michael V. Pak and Mark S. Gordon

Abstract

The reliability of spin polarization method results for atomic spin densities, obtained with several widely used Gaussian basis sets, is examined by comparison with the results of full configuration interaction (FCI) calculations. The spin densities obtained with these basis sets using the spin polarization model and some other methods disagree with the FCI treatment. Since the FCI wave function is exact for a given basis, it is not clear that the spin polarization model will be generally reliable. A large active space multi-configurational (CASSCF) calculation is shown to be inadequate as an alternative to FCI treatment. The importance of accounting at least to some extent for excitations to all orbitals in the complete space of basis functions is illustrated by very slow convergence of CASSCF results with increasing size of active space. The FCI results reported here can be used as benchmarks to test various approaches to spin density calculation.

1. Introduction

Electronic spin density at the positions of the nuclei determines the isotropic part of the interaction between the magnetic moments of the electron and the nuclei, also referred to as the Fermi contact interaction. Since this interaction is experimentally observable in electron paramagnetic resonance spectroscopy (EPS) as an isotropic hyperfine coupling constant (hfcc), calculation of the spin density at the nuclei is an important problem for electronic structure methods. It is also a difficult problem, because unlike most other electronic properties such as dipole moments, polarizabilities, etc. the hfcc's are determined by the amplitude of the wave function at a single point in space. However, in most quantum chemistry methods the wave function is found by optimization based on some global energy criterion. As a result, a variationally very good wave function may have significant error at some particular point in space.

The local character of the hfcc's makes the calculation very sensitive to the quality and size of the atomic basis. This sensitivity becomes extreme for systems in which unpaired electrons do not contribute directly to the spin density at the nuclei. For example, the unpaired electron in the ground state of boron atom occupies a p orbital having a node at the position of the nucleus, and thus cannot contribute directly to the spin density at the nucleus. The remaining s electrons do have non-zero density at the nucleus, but they all are paired. In this case the restricted open shell Hartree-Fock (ROHF) method predicts a value of zero for the isotropic hfcc, while experimentally it is equal to 12 MHz. This non-zero value is due to spin polarization contributions, resulting from nominally paired electrons having different exchange interactions with the unpaired electrons. A great number of open-shell radicals with an unpaired electron in a π-type orbital belong to this class of systems. This most difficult and arguably the most interesting case is the only type of hfcc calculations we will be concerned with here.

One way to describe the spin polarization effects is to use a spin-unrestricted Hartree-Fock wave function (UHF). The semiempirical INDO method, based on the UHF wave function, in many instances gives quantitative agreement with experiment [1]. A variety of ab-initio methods using UHF wave functions have been used to calculate hfcc's, sometimes giving very accurate results. Some of the methods included electron correlation, e.g. MBPT(4) [2], CCSD [2], QCISD [3]. The UHF-based methods also provide a physical explanation for often observed negative spin densities. However, the problem of spin contamination makes the use of any spin-unrestricted methods suspect, even if those methods include some procedures to remove the contamination (PUHF [4], UHF-AA [5]).

Another approach to describing the spin polarization effects requires construction of a multi-determinant wave function, to include all excitations accounting for orbital and spin polarization of s, p and sometimes d shells. This 'spin polarization' wave function is then optimized using some kind of MCSCF or CI procedures. An extensive review of the spin polarization method can be found in reference [6]. One important feature of this approach is the incomplete character of the wave function. Including into the wave function only those configurations which appear to be important according to a very simple physical picture of the phenomenon greatly simplifies the calculations; it also seems to allow a better understanding of the roles of different contributions to hfcc's. The latter problem has been a subject of thorough analysis, since it is relevant not only in the context of the spin polarization model, but also for various levels of CI treatment. In fact, the spin-polarized MCSCF (SP-MCSCF) and various CI methods alike take advantage of the idea that only some particular excitations are responsible for the spin density at the nucleus, while a great number of other configurations are unimportant in this respect and can be omitted from the wave function. A detailed discussion of the influence of various CI excitation classes on hfcc's can be found in

references [7,8], while references [6,9] deal with the same problem with respect to the SP-MCSCF approach. It should be noted that unlike the UHF treatment of spin polarization, all multi-determinant based methods account to some extent for true electron correlation effects, which are found to be significant for accurate description of hfcc's.

Unfortunately, many conclusions made regarding the role of various contributions to the spin density appear to be very much basis set dependent. When Gaussian basis sets are used for hfcc calculations, additional difficulty arises due to the fact that Gaussian functions, having zero radial slope at the nucleus, are unable to satisfy the correct cusp condition associated with the singularity of the Coulomb potential at the nucleus [10]. Slater-type orbitals, on the other hand, do have a cusp and can satisfy the cusp condition. However, using Slater-type orbitals (STO) instead of Gaussians for hfcc calculations, as suggested in reference [11] is generally not convenient, since most quantum chemistry programs currently available use Gaussian basis sets. Another approach, developed in reference [12] suggests expanding an STO basis set in Gaussian functions, calculating the wave functions with GTO's and then replacing the Gaussians with the corresponding STO's for the single purpose of hfcc evaluation, assuming no change in the expansion coefficients. This method, although quite effective, limits the choice of basis sets to be used in calculations to only those sets, for which STO-GTO conversion is available. The deficiency of Gaussian functions, on the other hand, does not necessarily make them unsuitable for hfcc calculations. In many simple cases, if the bulk of the spin density at the nucleus comes from an unpaired electron and the total value is relatively large, even small Gaussian basis sets do reproduce the experimental values for hfcc's. It has been shown that with very large Gaussian basis sets high accuracy can also be achieved for the most difficult systems, like a nitrogen atom [13].

An entirely different approach, initially suggested by Hiller, Sucher and Feinberg (HSF) [14] for the charge density, and later developed by Harriman [15] for spin density, substitutes a global operator for the local delta function type operator, thus avoiding most of the problems discussed above. With the recent development of HSF formalism to a more general class of global operators [16], this approach allows one to calculate hfcc's with high accuracy. Another advantage of this method is that unlike δ function based approaches it always gives better values for hfcc's as the wave function is variationally improved.

In view of the previous discussion, it is understandable that the choice of a method and a basis set for hfcc calculations can be a very confusing problem. There are numerous examples for which a particular CI expansion used together with some particular Gaussian basis set systematically give quite accurate values for hfcc's, whereas including more CI configurations into the wave function or using a larger basis set destroys the good agreement with experiment. For instance, a single excitations CI (S-CI) often gives very accurate hfcc's, but adding double excitations (SD-CI) leads to much poorer results [17]. A number of studies observed deterioration of results when larger and more flexible basis sets were used with the same computational method [11,12,17]. Several other examples of such 'paradoxical' behavior will be given in the present paper.

One possible way to analyze this problem is to separate the two main variables determining the accuracy of hfcc calculations - the size and flexibility of the basis set and the number and type of excitations to be included in the wave function. Since a full CI (FCI) calculation gives an exact wave function for a given basis set, the accuracy of hfcc's obtained by a FCI treatment reflects only the suitability of the basis set used in calculations, and not the sufficiency of the level of electron correlation. The suitability of various Gaussian basis sets for hfcc calculations has been a topic of several studies, with FCI 'calibration' calculations used as an

ultimate test [6,7,13]. Two of these works [7,13] address the nitrogen atom. Several Gaussian basis sets demonstrated to be inadequate for spin density calculations for N, however, are shown to perform well for other systems [6]. Among the first row atoms, nitrogen is perhaps the easiest system for spin density calculations (although it is much more difficult than most molecules).

In this work we calculate the FCI limit for hfcc's of the boron and carbon atom ground states, using a Gaussian basis set designed specifically for the purpose of spin density calculations [18]. The results in reference [18] are based entirely on the spin polarization model. Having the exact (FCI) spin densities allows us to place this method in perspective with regard to the suitability of various basis sets for hfcc calculations, and also provides one with a good benchmark for testing different approaches for these very difficult systems. The experimental values for boron and carbon are not well established [19]. Therefore, despite the deficiencies of our FCI results due to incompleteness of the basis sets used, they are nevertheless the best results currently available for these basis sets and as such can be used to test less computationally expensive methods.

2. Computational methods

In this work all calculations were performed using the GAMESS program [20]. The Gaussian basis sets used in the present work are those developed by Chipman [18]. These basis sets are various segmented contractions, suggested by Dunning [21], of the commonly used (9s5p) primitive Gaussian basis set of Huzinaga [22]. The changes suggested by Chipman include uncontracting the outer member of the innermost contraction and adding diffuse s and p functions and one or more d functions. For comparison, calculations were also done with the original Dunning basis sets, with and without diffuse sp and d polarization functions. A complete list of all basis sets employed in our calculations is

given in Table 1. The diffuse *sp* exponents used in all basis sets are (.0330 *s*, .0226 *p*) for boron and (.0479 *s*, .0358 *p*) for carbon. When only one set of d polarization functions is added to basis sets, its exponent is .32 for boron and .51 for carbon. When two sets of *d* functions are added, the exponents are (.1600, .6400) for boron and (.2800, 1.1200) for carbon.

It should be noted that Chipman's basis sets use 5-component spherical d functions instead of the 6 Cartesian components, and therefore all calculations were done with spherical functions. Using Cartesian d functions changes results significantly, since they essentially add an extra s function to the basis set.

Full CI calculations with the basis sets discussed above result in CI expansions containing millions of determinants and were greatly facilitated by using a very fast determinant-based CI code written by Ivanic and Ruedenberg [23].

Since electronic ground states of B and C atoms are ^2P and ^3P respectively, in all complete active space self-consistent field (CASSCF) calculations reported in this work, the electron density was averaged over all degenerate states, to ensure that the resulting wave function was a true $\hat{L}^2$ (angular momentum) eigenfunction.

3. Results and discussion

As noted in the Introduction, FCI provides the ultimate test of the suitability of an atomic orbital (AO) basis set for spin density calculations. FCI spin densities are essentially of benchmarking value; if any other method gives better results for spin densities using the same basis set, these results are likely to be due to fortuitous cancellation of errors. In this work we report FCI spin densities in boron and carbon atoms, obtained with several basis sets commonly used for spin density calculations. Table 2 contains total energies and spin densities for boron, Table 3 presents the same data for carbon. The best available experimental spin densities are

0.0081 for boron [24] and 0.0173 for carbon [25]. Our choice of Chipman's Gaussian basis sets for this study was prompted by the illustration [18,26] that these basis sets are capable of providing a reasonably good description of Fermi contact spin densities. The last column of the tables gives the spin density obtained by Chipman [18] using the corresponding basis sets and the spin polarization MCSCF model discussed above.

For each basis set studied, adding diffuse *sp* functions and then one or two *d* functions results in a continuous increase of the spin density at the nucleus. All sequences appear to converge to values considerably different from the experimental spin densities, even in the case of the [6s,3p]+*sp*+*dd* basis set specifically designed for spin density calculations. For carbon, even with a single *d* function FCI considerably overestimates the correct value for the spin density. It is reasonable to expect [13,18] that adding the second and then the third *d* function to the basis set would further increase the spin density, thus making the results even less accurate.

The results of spin polarization calculations apparently do not agree well with the FCI limit, and there appears to be no systematic dependence on the way in which the results of these two methods differ. This would suggest that the spin polarization model overlooks some excitations that are important for a correct description of the spin density at the nuclei. On the other hand, the highly unsatisfactory results of FCI calculations suggest that the basis sets considered here are inadequate for the task; therefore, spin density obtained with these basis sets must be considered suspect. Since these basis sets approach the accuracy of a complete basis set within the spin polarization model [18], the current results illustrate the inadequacy of this level of theory.

One alternative to FCI is a smaller CI expansion. For nitrogen atom, which is a much simpler system with respect to spin density calculations than boron or carbon [19,27], it was demonstrated that at least quadruple excitations are required if a single reference wave function is used. A multi-

reference CI wave function based on a relatively small CASSCF reference function predicts a N spin density that is very close to FCI [13,28]. There is a number of studies of the relative roles of single, double, triple and higher excitations available in literature [7,8]. In this work we take a different approach and investigate the convergence of spin density with increasing size of the CASSCF active space. In other words, instead of including a limited number of excitations within the space spanned by all basis functions, we include all excitations within a smaller space, and then gradually increase the size of that active space, up to FCI. It should be emphasized that we use a complete active space wave function, which includes all excitations within the active space. This is quite different from the spin polarization MCSCF wave function, which includes only a limited number of spin polarization configurations. The results of these CASSCF-based calculations for the [5's,2p]+sp +d (d exponent 0.40) basis set are given in Table 4.

As can be seen from the table, the convergence of the spin density is very slow; the CASSCF value for an active space which is only three orbitals short of the full space is still 20% off the FCI value. It appears that at least some excitations to orbitals of very high orbital momentum should be included in the wavefunction [29], and therefore we are forced to conclude that CASSCF calculations probably can not be used as a substitute for FCI.

4. Conclusions

It appears that the basis sets studied in this work are largely inadequate for calculation of spin densities at the nuclei, at least in case of boron and carbon atoms. The results obtained with these basis sets using the spin polarization model and some other methods disagree with the FCI treatment. Since the FCI wave function is exact for a given basis, it is not clear that the spin polarization model will be generally reliable. It is unlikely that a method that does not account at least to some extent for

excitations to all orbitals in the complete space of basis functions would be successful in correctly describing atomic spin densities at the nuclei. Including excitations within only a subspace of the complete space is not sufficient, even if all such excitations are included. This is illustrated by very slow convergence of CASSCF results with increasing size of active space. The FCI results reported in this work can be used as benchmarks to test various approaches to spin density calculation.

References

1. J.A.Pople, D.L.Beveridge, P.A.Dobosh, J.Amer.Chem.Soc. **90**, 4201 (1968)

2. H.Sekino, R.J.Bartlett, J.Chem.Phys. **82**, 4225 (1985)

3. I.Carmichael, J.Phys.Chem. **95**, 108 (1991)

4. J.Harriman, J.Chem.Phys. **40**, 2827 (1964)

5. A.T.Amos, L.C.Snyder, J.Chem.Phys. **41**, 1773 (1964)

6. D.M.Chipman, Theor.Chim.Acta. **82**, 93 (1992)

7. B.Engels, S.D.Peyerimhoff, E.R.Davidson, Mol.Phys. **62**, 109 (1987)

8. B.Engels, L.Eriksson, S.Lunell, Adv.Quant.Chem. **27**, 297 (1996)

9. D.M.Chipman, Phys.Rev. A **39**, 475 (1989)

10. T.Kato, Commun.Pure Appl.Math. **10**, 151 (1957)

11. D.Feller, E.R.Davidson, J.Chem.Phys. **80**, 1006 (1984)

12. H.Nakatsuji, M.Izawa, J.Chem.Phys. **91**, 6205 (1989)

13. C.W.Bauschlicher, S.R.Langhoff, H.Partridge, D.P.Chong, J.Chem.Phys. **89**, 2985 (1988)

14. J.Hiller, J.Sucher, G.Feinberg, Phys.Rev. A **18**, 2399 (1978)

15. J.E.Harriman, Int.J.Quant.Chem. **17**, 689 (1980)

16. V.A.Rassolov, D.M.Chipman, J.Chem.Phys. **105**, 1470 (1996)

17. D.Feller, E.R.Davidson, Theor.Chim.Acta. **68**, 57 (1985)

18. D.M.Chipman, Theor.Chim.Acta. **76**, 73 (1989)

19. I.Carmichael, J.Phys.Chem. A **101**, 4633 (1997)

20. M.W.Schmidt, K.K.Baldridge, J.A.Boatz, S.T.Elbert, M.S.Gordon, J.H.Jensen, S.Koseki, N.Matsunaga, K.A.Nguyen, S.J.Su, T.L.Windus, M.Dupuis, J.A.Montgomery, J.Comp.Chem. **14**, 1347 (1993)

21. T.H.Dunning, J.Chem.Phys. **53**, 2823 (1970)

22. S.Huzinaga, J.Chem.Phys. **42**, 1293 (1965)

23. J.Ivanic, K.Ruedenberg, to be published

24. J.S.M.Harvey, L.Evans, H.Lew, Can.J.Phys. **50**, 1719 (1972)

25. I.Carmichael, J.Chem.Phys. **95** 108 (1991)

26. D.M.Chipman, J.Chem.Phys. **91**, 5455 (1989)

27. D.Feller, E.R.Davidson, J.Chem.Phys. **88**, 7580 (1988)

28. C.W.Bauschlicher, J.Chem.Phys. **92**, 518 (1990)

29. I.Carmichael, private communication

Table 1. Gaussian basis sets used for spin density calculations
in boron and carbon atoms.

Basis set	Reference
[4s,2p], [5s,3p]	[21]
[4s,2p], [5s,3p] + diff *sp*, [4s,2p], [5s,3p] + diff *sp* + *d*	[18]
[5s',2p], [6s,3p]	[18]
[5s',2p], [6s,3p] + diff *sp* + *d*, [5s',2p], [6s,3p] + diff *sp* + *dd*	[18]

Table 2. Full CI spin density of boron atom
calculated with various basis sets.

	Total energy (a.u.) (FCI)	Spin density (a.u.) (FCI)	Spin density (a.u.) (SP MCSCF)[1]
[4s,2p]	-24.582402	-.0008180	-.0019
[4s,2p]+*sp*	-24.582889	-.0005524	
[4s,2p]+*sp+d*	-24.603558	.0163919	
[4s,2p]+*sp+dd*	-24.606311	.0190476	
[5's,2p][2]	-24.583794	-.0128072	
[5's,2p]+*sp*	-24.584257	-.0098031	-.0079
[5's,2p]+*sp+d*	-24.604987	.0091495	
[5's,2p]+*sp+dd*	-24.607736	.0112065	
[5s,3p]	-24.587073	.0094219	.0133
[5s,3p]+*sp*	-24.587435	.0091669	.0132
[5s,3p]+*sp+d*	-24.608220	.0268019	
[5s,3p]+*sp+dd*	-24.611127	.0290120	
[6s,3p]	-24.589024	-.0214443	
[6s,3p]+*sp*	-24.589309	-.0172626	-.0079
[6s,3p]+*sp+d*	-24.610144	.0041297	.0140
[6s,3p]+*sp+dd*	-24.613042	.0055280	.0143

[1]Spin polarization MCSCF results [18]

[2]Notation introduces by Chipman and described in reference [18]

Table 3. Full CI spin density of carbon atom
calculated with various basis sets.

	Total energy (a.u.) (FCI)	Spin density (a.u.) (FCI)	Spin density (a.u.) (SP MCSCF)
[5's,2p]	-37.738055	.0014321	
[5's,2p]+*sp*	-37.739280	.0163082	.0012
[5's,2p]+*sp*+*d*	-37.778178	.0359382	
[5's,2p]+*sp*+*dd*	-37.784688	.0415749	
[5s,3p]	-37.744352	.0692087	.0331
[5s,3p]+*sp*	-37.745363	.0749169	.0340
[5s,3p]+*sp*+*d*	-37.784815	.0935047	
[5s,3p]+*sp*+*dd*	----[1]	----	
[6s,3p]	-37.746956	-.0235588	
[6s,3p]+*sp*	-37.747824	-.0041899	.0018
[6s,3p]+*sp*+*d*	-37.787278	.0234380	.0198
[6s,3p]+*sp*+*dd*	----	----	.0212

[1] Too large to permit FCI calculations

Table 4. Convergence of CASSCF spin density with increasing size of active space: from small CASSCF to full CI (all electrons included)

	E(CASSCF)	Spin Density
MCSCF(9) 1s2s2p3s3p	-24.570213	.0451845
MCSCF(13) 1s2s2p3s3p4p4s	-24.583678	-.0132546
MCSCF(14) 1s2s2p3s3p4p4s5s	-24.584180	-.0099208
MCSCF(15) [1s2s2p]3s3p4s3d	-24.604076	-.0056539
MCSCF(18) 1s2s2p3s3p4p4s3d	-24.604223	-.0057322
MCSCF(19) 1s2s2p3s3p4p4s3d5s	-24.604663	-.0011207
FCI=MCSCF(22) 1s2s2p3s3p4p4s3d5s6p	-24.604715	-.0009381

CHAPTER 4: MCQDPT HYPERFINE COUPLING TENSOR

Michael V. Pak and Mark S. Gordon

1. Introduction

There are two main reasons why multi-reference methods are crucial for calculating spin-spin coupling. First, as was discussed in chapter 2, single-reference methods can be very unreliable for calculating the spin-spin coupling constants, due to the triplet nature of perturbing operators [1]. In general, for molecules without multiple bonds or lone pairs the spin-spin coupling constants can be calculated with reasonable accuracy with Hartree-Fock based methods, while single-reference calculations of coupling to nuclei with lone pairs can be in error by orders of magnitude [1-3]. In principle, this particular problem can be dealt with by using a UHF wave function, which usually contains some contributions from the triplet and higher spin states. However, systems involving degenerate or nearly degenerate configurations cannot be adequately studied with any single-reference methods, including UHF [4]. The MCSCF wave function is much better suited for describing systems in which non-dynamic correlation is important. The MCSCF wave function is also flexible enough to properly accommodate the effects of operators responsible for indirect spin-spin coupling [1]. However, it is important to recall that while MCSCF is a generalization of Hartree-Fock theory for systems that are not well described by a single configuration, it

does not account for dynamic correlation effects. At present, analytic calculation of spin-spin coupling is available for MCSCF theory itself [5], but not to our knowledge for any MCSCF based methods that include dynamic correlation.

Direct analytic calculation of spin-spin coupling constants for MCQDPT theory appears to be prohibitively difficult. Since MCQDPT theory is not variational, calculating even the first derivatives of the MCQDPT energy requires evaluation of the responses of the MCQDPT wave function. However, even deriving the response equations is very complicated due to the specific nature of some of the MCQDPT optimization parameters, such as the energy shifts and the MCQDPT orbital energies discussed below. If the response function formalism is used, solving response equations is not necessary for the first derivatives, but is required for the spin-spin coupling constants, which are the second derivatives of the energy with respect to the magnetic moments. A combined analytical – numerical approach seems to be more practical. In this approach, the first derivatives of the MCQDPT energy with respect to the nuclear magnetic moments (hyperfine coupling tensors) are calculated analytically, using the variational Lagrangian technique described below. These gradients can then be numerically differentiated to obtain the spin-spin coupling constants. A similar approach is frequently used in electronic structure codes for calculating numerical Hessians by numerical differentiation of analytic energy gradients.

In this chapter, a derivation of the analytic gradient with respect the nuclear magnetic moments for MCQDPT theory is presented. This derivation is original, although the first half follows closely the derivation of the only other kind of analytic gradients available for MCQDPT theory – with respect to nuclear coordinates, developed by Nakano, Hirao and Gordon [6,7].

2. Derivatives for non-variational wave functions

The difficulty of calculating magnetic and other properties for MCQDPT theory lies in the non-variational character of the MCQDPT energy. This can be illustrated by the following example. Consider the hyperfine coupling tensor

$$A_K = \frac{dE}{dM_K} \tag{1}$$

For simplicity, we ignore the details of the parametrization of the electronic energy E and write the energy functions as $E(M,\lambda)$, where M represents the nuclear magnetic moments and $\lambda=\{\lambda_i\}$ is the set of all parameters that determine the wave function. The gradient of the electronic energy with respect to the magnetic moment of nucleus K, calculated for variationally optimal values of the electronic parameters $\lambda=\lambda^*$ is

$$\frac{dE(M,\lambda)}{dM_K} = \left[\frac{\partial E(M,\lambda)}{\partial M_K} + \sum_i \frac{\partial E(M,\lambda)}{\partial \lambda_i} \frac{\partial \lambda_i}{\partial M_K} \right]_{\lambda=\lambda^*} \tag{2}$$

If the electronic energy is fully variational with respect to all the optimization parameters λ, the optimized energy satisfies the variational condition

$$\left[\frac{\partial E(M,\lambda)}{\partial \lambda} \right]_{\lambda=\lambda^*} = 0 \tag{3}$$

for all values of the nuclear magnetic moments M, and the hyperfine coupling tensor does not depend on the response of the optimization parameters $\partial\lambda/\partial M_K$:

$$A_K = \left[\frac{\partial E(M,\lambda^*)}{\partial M_K} \right]_{M=0} \tag{4}$$

The expressions for second order properties, such as spin-spin coupling constants, are also simplified greatly if the variational condition (3) is satisfied.

However, if the parameters λ are not determined variationally, the condition Eq.(3) is not satisfied, and one needs to evaluate the responses of the wave function even for first order properties. Obtaining these responses also becomes a much more difficult task, since one can no longer rely on the variational condition Eq. (3) to derive the response equations. To deal with these problems, it was suggested by Helgaker and Jørgensen [8,9] to apply Lagrange's method of undetermined multipliers and to introduce an energy functional which would give the same energy as the standard energy function and yet be fully variational.

In non-variational methods, the optimization parameters λ are determined not from the variational condition Eq.(3) but from some set of equations $f(\lambda)=0$, and then the optimized values λ_{opt} are used to calculate the electronic energy $E(\lambda_{opt})$. A variational functional (Lagrangian) can be constructed by introducing an additional set of optimization parameters μ, including one parameter for each of the optimization conditions $f(\lambda)=0$:

$$L(\lambda,\mu) = E(\lambda) + \mu f(\lambda) \qquad (5)$$

This Lagrangian is variational with respect to the new parameters μ. In fact, the variational conditions for the Lagrangian with respect to the μ's are identical to the set of equations $f(\lambda)=0$, from which the optimal values of parameters λ are determined:

$$\frac{\partial L(\lambda,\mu)}{\partial \mu} = f(\lambda) = 0 \qquad (6)$$

On the other hand, the parameters μ are arbitrary, since for the optimized values of $\lambda=\lambda_{opt}$ the last term in Eq. (5) vanishes, and $L(\lambda_{opt},\mu) = E(\lambda_{opt})$ for any value of μ. Thus, it is possible to make the Lagrangian fully variational in both sets of parameters λ and μ by imposing a constraining condition on the μ's:

$$\frac{\partial L(\lambda,\mu)}{\partial \lambda} = \frac{\partial E(\lambda)}{\partial \lambda} + \mu \frac{\partial f(\lambda)}{\partial \lambda} = 0 \qquad (7)$$

The set of equations (7) represents variational conditions for the Lagrangian with respect to parameters λ. However, it should be emphasized that by solving Eq. (7) the optimal values μ_{opt} of parameters μ are found, while the optimal values of parameters λ are found from variational conditions of the Lagrangian with respect to the μ's Eq. (6). If parameters λ are determined from Eq. (6), and parameters μ - from Eq. (7), the Lagrangian yields the same energy as the original energy functional $E(\lambda)$, and at the same time it is variational with respect to all optimization parameters:

$$\begin{cases} L(\lambda_{opt}, \mu_{opt}) = E(\lambda_{opt}) \\ \dfrac{\partial L(\lambda,\mu)}{\partial \lambda} = 0 \\ \dfrac{\partial L(\lambda,\mu)}{\partial \mu} = 0 \end{cases} \qquad (8)$$

This Lagrangian can now be used in place of the original energy functional to calculate various energy derivatives through the standard response function formalism.

3. MCQDPT magnetic gradients – general strategy

Consider the main steps involved in calculating the hyperfine coupling tensors analytically. First, a variational functional is constructed, which requires identifying all of the optimization parameters in the energy expression and the corresponding equations for these parameters. The Lagrange multipliers are determined by solving the variational equations (7). Since these equations are solved for zero magnetic moments, it is not necessary to include in the energy function E the perturbation due to the presence of the nuclear magnetic moments M at this stage:

$$\frac{\partial L(M,\lambda,\mu)}{\partial \lambda}\bigg|_{M=0} = \frac{\partial L(\lambda,\mu)}{\partial \lambda} = \frac{\partial E(\lambda)}{\partial \lambda} + \mu\frac{\partial f(\lambda)}{\partial \lambda} = 0 \qquad (8)$$

As a result, the set of equations (8) is identical to the set of equations used in ref. [6] for MCQDPT gradients with respect to nuclear coordinates. However, not all of the equations (8) need to be solved, because not all of the Lagrangian multipliers are necessary for calculating the magnetic gradients:

$$\frac{dL(M,\lambda_{opt},\mu_{opt})}{dM_K}\bigg|_{M=0} = \left[\frac{\partial L(M,\lambda,\mu)}{\partial M_K} + \frac{\partial L(M,\lambda,\mu)}{\partial \lambda}\frac{\partial \lambda}{\partial M_K} + \frac{\partial L(M,\lambda,\mu)}{\partial \mu}\frac{\partial \mu}{\partial M_K}\right]_{\substack{\lambda=\lambda_{opt}\\ \mu=\mu_{opt}\\ M=0}}$$

$$= \left[\frac{\partial L(M,\lambda,\mu)}{\partial M_K}\right]_{\substack{\lambda=\lambda_{opt}\\ \mu=\mu_{opt}\\ M=0}} = \left[\frac{\partial E(M,\lambda)}{\partial M_K} + \mu\frac{\partial f(M,\lambda)}{\partial M_K}\right]_{\substack{\lambda=\lambda_{opt}\\ \mu=\mu_{opt}\\ M=0}} \qquad (9)$$

Indeed, if some of the constraining conditions $f(M, \lambda)$ in Eq.(9) do not depend explicitly on the nuclear magnetic moments, their derivatives with respect to M_K are equal to zero, and we don't need the corresponding Lagrange multipliers μ to calculate the gradient.

The next step involves calculating the derivatives of the optimization equations $f(M, \lambda)$ and the energy function $E(M, \lambda)$ with respect to the nuclear magnetic moments. It should be noted that we only need the derivatives of those optimization equations that correspond to non-zero Lagrange multipliers. If some Lagrange multipliers μ associated with constraining conditions $f(M, \lambda)$ happen to be equal to zero, the corresponding contributions $\mu\frac{\partial f(M,\lambda)}{\partial M_K}$ to the derivative of the Lagrangian in Eq.(9) are also automatically equal to zero, and hence the derivatives of those particular constraining conditions $\frac{\partial f(M,\lambda)}{\partial M_K}$ need not be calculated. Finally, the gradients are computed using these derivatives and the Lagrange multipliers obtained from variational conditions Eq. (8).

4. MCQDPT Lagrangian

All derivations in this Section and Section 5 are analogous to the results of Nakano, Hirao and Gordon [6]. The MCQDPT total energy to second order can be written as

$$E = \sum_{\alpha\beta} D_\alpha D_\beta (H_{eff})_{\alpha\beta} / \sum_\alpha D_\alpha^2 \qquad (10)$$

where H_{eff} is the effective Hamiltonian and D_α are elements of the eigenvectors which diagonalize it. The effective Hamiltonian is given by

$$(H_{eff})_{\alpha\beta} = <\alpha|H|\beta> + \frac{1}{2}\left\{ \sum_K \frac{<\alpha|V|K><K|V|\beta>}{E_\alpha^{(0)} - E_K^{(0)}} + (\alpha \leftrightarrow \beta)\right\} \qquad (11)$$

where the sum is over the set of all singly and doubly excited configurations K from the reference configurations in the complete active space (CAS). The vectors $|\alpha>$ and $|\beta>$ are CASSCF eigenfunctions. As was mentioned earlier, the Hamiltonian operator H does not contain any contributions from nuclear magnetic moments at this stage. The perturbation operator V of the MCQDPT theory [10-11] in second-quantized form is

$$V = \sum_{pq}(h_{pq} - \varepsilon_p \delta_{pq})E_{pq} + \frac{1}{2}\sum_{pqrs}(pq|rs)E_{pq,rs} \qquad (12)$$

where E_{pq} are unitary group generators defined in terms of the creation operators $a_{p\alpha}^+$, $a_{p\beta}^+$ and annihilation operators $a_{p\alpha}$, $a_{p\beta}$ associated with molecular orbitals p, q with spins α, β:

$$E_{pq} = a_{p\alpha}^+ a_{q\alpha} + a_{p\beta}^+ a_{q\beta} \qquad (13)$$

and $h_{pq} = (p|h|q)$ are the elements of the one-electron Hamiltonian matrix in the molecular orbital basis. The orbital energies ε_p in the MCQDPT theory are uniquely defined by orbital canonicalization, and are important parameters of the MCQDPT perturbation operator. In the two-electron part of the perturbation, $E_{pq,rs} = E_{pq}E_{rs} - \delta_{qr}E_{ps}$, and $(pq|rs)$ are the four index matrix

elements   of   the   electron-electron   repulsion

$(pq\,|\,rs)=\iint dr_1 dr_2 \varphi_p^*(r_1)\varphi_r^*(r_2)\dfrac{1}{r_{12}}\varphi_q(r_1)\varphi_s(r_2)$. Using the relations [6]

$$E_{pq,rs,tu} = E_{pq,rs}E_{tu} - \delta_{qt}E_{pu,rs} - \delta_{st}E_{pq,ru} \tag{14}$$

and introducing the one-electron perturbation operator v with matrix elements defined as $(p\,|\,v\,|\,q)=(p\,|\,h\,|\,q)-\varepsilon_p\delta_{pq}$, an expanded expression for the effective Hamiltonian can be written:

$$
\begin{aligned}
(H_{e\!f\!f})_{\alpha\beta} =&<\alpha\,|\,H\,|\,\beta> -\frac{1}{2}\Bigg\{\sum_{pq,B}<\alpha\,|\,E_{pq}\,|\,B>C_B(\beta)\sum_e\frac{(p\,|\,v\,|\,e)(e\,|\,v\,|\,q)}{\varepsilon_e-\varepsilon_q+\Delta E_{B\alpha}}\\
&-\sum_{pqrs,B}<\alpha\,|\,E_{pq,rs}\,|\,B>C_B(\beta)\Bigg[\sum_e\frac{(p\,|\,v\,|\,e)(eq\,|\,rs)}{\varepsilon_e-\varepsilon_q+\varepsilon_r-\varepsilon_s+\Delta E_{B\alpha}}+\sum_e\frac{(pe\,|\,rs)(e\,|\,v\,|\,q)}{\varepsilon_e-\varepsilon_q+\Delta E_{B\alpha}}\\
&+\frac{1}{2}\sum_{(a,b)}\frac{(pa\,|\,rb)(aq\,|\,bs)}{\varepsilon_a-\varepsilon_q+\varepsilon_b-\varepsilon_s+\Delta E_{B\alpha}}\Bigg]\\
&-\sum_{pqrstu,B}<\alpha\,|\,E_{pq,rs,tu}\,|\,B>C_B(\beta)\sum_e\frac{(pe\,|\,rs)(eq\,|\,tu)}{\varepsilon_e-\varepsilon_q+\varepsilon_t-\varepsilon_u+\Delta E_{B\alpha}}+(\alpha\leftrightarrow\beta)\Bigg\}
\end{aligned}
\tag{15}
$$

In Eq.(15), B refers to a configuration state function (CSF) in the CASSCF wave function and $C_B(\beta)$ is a CASSCF CI coefficient for the CSF B in state β. Active orbitals have indices p,q,r,s,t,u and the virtual orbitals are indicated by indices e,f. Indices a,b refer to both active and virtual orbitals, but a and b cannot both be virtual orbitals simultaneously. The energy shift $\Delta E_{B\alpha}$ is the difference between the energies of the MCSCF state α and CSF B.

The optimization parameters in MCQDPT theory are the molecular orbital coefficients, MCSCF orbital energies (uniquely defined by orbital canonicalization) and MCSCF CI coefficients. These parameters are determined by the MCSCF orbital canonicalization conditions, which are used as constraining conditions to build the MCQDPT Lagrangian. Following

Nakano et al. [6], the equations for the optimization parameters are listed here in the order they are determined in the MCQDPT calculation.

First, the CI and molecular orbital coefficients are found by solving the MCSCF equations. The CI coefficients for the MCSCF state α are determined from the MCSCF Hamiltonian diagonalization

$$\sum_B (H_{AB} - \delta_{AB} E^{CAS}(\alpha)) C_B(\alpha) = 0; \qquad \sum_B C_B^2(\alpha) = 1 \qquad (16)$$

The variational conditions for the molecular orbital coefficients can be written as symmetry conditions $X_{pq} = X_{qp}$ for the state-averaged matrix X defined as

$$X_{pq} = \sum_\alpha \omega(\alpha) X_{pq}(\alpha) = \sum_\alpha \omega(\alpha) \left[\sum_i h_{pi} < \alpha \mid E_{qi} \mid \alpha > + \frac{1}{2} \sum_{ijk} (pi \mid jk) < \alpha \mid E_{qi,jk} \mid \alpha > \right] (17)$$

where $\omega(\alpha)$ is the weight of the MCSCF state α. Using pure state MCSCF wave function somewhat simplifies the derivation. However, if the MCSCF states are degenerate, averaging over several MCSCF states can be important for calculation of molecular properties, and thus for generality a state-averaged MCSCF wave function is used in this work.

The orthonormality conditions for the molecular orbitals $(p \mid q) = \delta_{pq}$ implied in the MCSCF orbital optimization, have to be included in the Lagrangian explicitly.

The MCSCF optimization determines molecular orbitals not uniquely, but up to arbitrary rotations within either the doubly occupied, active or virtual orbital subspaces. The MCQDPT energy is not invariant with respect to such rotations, and this rotational freedom of MCSCF orbitals has to be removed by orbital canonicalization, which can be thought of as the diagonalization of the MCSCF Fock matrix. The canonicalization conditions also uniquely define the orbital energies used in the MCQDPT energy functional. These conditions can be written as

$$F_{pq} - \varepsilon_p \delta_{pq} = (p|h|q) + \sum_{rs} D_{rs}^{Ave}[(pq|rs) - \frac{1}{2}(pr|sq)] - \varepsilon_p \delta_{pq} = 0 \qquad (18)$$

Here D^{Ave} is the state averaged density matrix

$$D_{pq}^{Ave} = \sum_\alpha \omega(\alpha) < \alpha | E_{pq} | \alpha > \qquad (19)$$

and each block (doubly occupied, active and external) of the Fock matrix F_{pq} is diagonalized separately.

The last set of MCQDPT optimization parameters comes from diagonalization of the effective Hamiltonian

$$\sum_\beta ((H_{eff})_{\alpha\beta} - \delta_{\alpha\beta}E)D_\beta = 0; \qquad \sum_\alpha D_\alpha^2 = 1 \qquad (20)$$

Introducing one Lagrange multiplier μ for each of the constraining conditions described above, one can write the MCQDPT Lagrangian as

$$L = \left[\sum_{\alpha\beta} D_\alpha D_\beta (H_{eff})_{\alpha\beta} / \sum_\alpha D_\alpha^2 \right] + \left[\sum_\alpha \sum_A \mu_{CASCI}^{A\alpha} \left\{ \sum_B (H_{AB} - \delta_{AB}E^{CAS}(\alpha))C_B(\alpha) \right\} \right.$$

$$+ \sum_\alpha \mu_{CAS}^\alpha \left\{ \sum_A C_A^2(\alpha) - 1 \right\} + \sum_{p>q \in O} \mu_{CASMO}^{pq} \left\{ X_{pq} - X_{qp} \right\} + \sum_{p \geq q \in D} \mu_{CASMO}^{pq} \left\{ F_{pq} - \varepsilon_p \delta_{qp} \right\} \qquad (21)$$

$$+ \sum_{p \geq q} \mu_{ORTMO}^{pq} \left\{ (p|q) - \delta_{pq} \right\} + \sum_\alpha \mu_H^\alpha \left\{ \sum_\beta (H_{eff})_{\alpha\beta} D_\beta - ED_\alpha \right\} + \mu_H \left\{ \sum_\alpha D_\alpha^2 - 1 \right\} \right]$$

Here the summation over $p > q \in O$ means that orbitals p and q are in different orbital subspaces (doubly occupied, active or virtual), and the sum over $p \geq q \in D$ indicates that both orbitals belong to the same orbital subspace. The procedures for determining the Lagrange multipliers μ in Eq.(21) are discussed in the following section.

5. Lagrange multipliers

The Lagrange multipliers μ are calculated from variational conditions Eq.(8). However, in order to compute the derivatives of the Lagrangian, each

μ is to be multiplied by the derivative of the corresponding constraining condition

$$\frac{dL(M,\lambda_{opt},\mu_{opt})}{dM_K}\bigg|_{M=0} = \left[\frac{\partial E(M,\lambda_{opt})}{\partial M_K} + \mu_{opt}\frac{\partial f(M,\lambda_{opt})}{\partial M_K}\right]_{M=0} \quad (22)$$

Therefore, it is not necessary to calculate those multipliers for which $\frac{\partial f(M,\lambda_{opt})}{\partial M_K}\bigg|_{M=0} = 0$. It follows from Eq.(21) that the multipliers μ^{α}_{CAS}, μ^{pq}_{ORTMO} and μ_H need not be calculated, since none of the orthonormalization conditions depends explicitly on the magnetic moments of the nuclei.

Furthermore, for the optimized values of D_α, the MCQDPT energy is stationary with respect to any changes in D_α, and since $\frac{\partial E(\lambda_{opt})}{\partial D_\alpha} = 0$, the variational condition Eq.(8) for μ^{α}_H has the solution $\mu^{\alpha}_H = 0$. This means that only three kinds of Lagrange multipliers: $\mu^{A\alpha}_{CASCI}$ and the two types of μ^{pq}_{CASMO}, need to be evaluated to calculate the derivatives of the Lagrangian with respect to the nuclear magnetic moments:

$$\frac{dL(M,\lambda_{opt},\mu_{opt})}{dM_K}\bigg|_{M=0} = \left[\left(\sum_{\alpha\beta}D_\alpha D_\beta\frac{\partial(H_{eff})_{\alpha\beta}}{\partial M_K}\bigg/\sum_{\alpha}D_\alpha^2\right) + \sum_{\alpha}\sum_{A}\mu^{A\alpha}_{CASCI}\sum_{B}\frac{\partial H_{AB}}{\partial M_K}C_B(\alpha)\right.$$
$$\left. + \sum_{p>q\in O}\mu^{pq}_{CASMO}\frac{\partial}{\partial M_K}\{X_{pq}-X_{qp}\} + \sum_{p\geq q\in D}\mu^{pq}_{CASMO}\frac{\partial F_{pq}}{\partial M_K}\right]_{M=0} \quad (23)$$

The equations for evaluating these multipliers were derived by Nakano et al. [6]. The multipliers for the MO rotations mixing different subspaces and for the CI coefficients are obtained by solving coupled linear equations corresponding to the state-averaged CASSCF equations (see Eq.(43) in ref. [6]). The multipliers corresponding to the canonicalization procedure for the doubly occupied and external subspaces can be determined without having to solve linear equations, and a small set of linear equations of dimension

$n_{act}(n_{act}-1)/2$, where n_{act} is the number of active orbitals, must be solved to obtain multipliers for the active subspace (Eq.(41) in ref. [6]).

6. Derivatives of the constraining conditions

The derivatives of the Lagrangian with respect to the nuclear magnetic moments (Eq. (23)) are determined by the derivative of the MCQDPT effective Hamiltonian $\dfrac{\partial(H_{eff})_{\alpha\beta}}{\partial M_K}$, as well as by the following three derivatives of

constraining conditions: $\dfrac{\partial H_{AB}}{\partial M_K}$, $\dfrac{\partial}{\partial M_K}\{X_{pq} - X_{qp}\}$ and $\dfrac{\partial F_{pq}}{\partial M_K}$. The evaluation of

these derivatives is relatively straightforward.

As was shown in chapter 2, differentiating the non-relativistic Hamiltonian with respect to the nuclear magnetic moment M_K results in the hyperfine operator

$$\frac{dH}{dM_K} = H_K = H_K^{PSO} + H_K^{SD} + H_K^{FC} \tag{24}$$

where H_K^{PSO}, H_K^{SD} and H_K^{FC} are the paramagnetic spin-orbit, the spin-dipole and the Fermi contact operators accordingly. These operators and the corresponding one-electron hyperfine operators h_K are discussed in detail in chapter 2.

The first term in the expression for the MCQDPT hyperfine coupling tensor Eq.(23) is the derivative of the MCQDPT energy. Introducing the matrix elements of the one-particle perturbation $h_K^{pq} = (p|h_K|q)$, the derivative of the effective Hamiltonian can be written as

$$\frac{\partial (H_{eff})_{\alpha\beta}}{\partial M_K} = <\alpha|H_K|\beta> -\frac{1}{2}\left\{\sum_{pq,B}<\alpha|E_{pq}|B>C_B(\beta)\left[\sum_e\frac{h_K^{pe}(e|v|q)}{\varepsilon_e-\varepsilon_q+\Delta E_{B\alpha}}\right.\right.$$

$$\left.+\sum_e\frac{h_K^{eq}(p|v|e)}{\varepsilon_e-\varepsilon_q+\Delta E_{B\alpha}}\right]-\sum_{pqrs,B}<\alpha|E_{pq,rs}|B>C_B(\beta)\left[\sum_e\frac{h_K^{pe}(eq|rs)}{\varepsilon_e-\varepsilon_q+\varepsilon_r-\varepsilon_s+\Delta E_{B\alpha}}\right. \qquad (25)$$

$$\left.\left.+\sum_e\frac{h_K^{eq}(pe|rs)}{\varepsilon_e-\varepsilon_q+\Delta E_{B\alpha}}\right]+(\alpha\leftrightarrow\beta)\right\}$$

Evaluation of $<\alpha|H_K|\beta>$ in Eq.(25) involves calculation of the matrix elements $<A|H_K|B>$ of the hyperfine operator H_K for two CSF's $|A>$ and $|B>$ belonging to two different CASSCF states $|\alpha>$ and $|\beta>$:

$$<\alpha|H_K|\beta> = \sum_{A,B}C_A(\alpha)C_B(\beta)<A|H_K|B> \qquad (26)$$

The derivative of the constraining condition for the CI coefficients is $\sum_B\frac{\partial H_{AB}}{\partial M_K}C_B(\alpha)$, where $\frac{\partial H_{AB}}{\partial M_K}$ is simply the matrix element $<A|H_K|B>$ of the hyperfine operator H_K for two CSF's in the same CASSCF eigenfunction.

Calculation of the derivatives of the remaining two constraining conditions $\frac{\partial}{\partial M_K}\{X_{pq}-X_{qp}\}$ and $\frac{\partial F_{pq}}{\partial M_K}$ requires evaluation of the matrix elements of the one-particle hyperfine operator h_K^{pq}, already used for calculating the MCQDPT energy derivative Eq.(25):

$$\frac{\partial F_{pq}}{\partial M_K}=h_K^{pq} \qquad \frac{\partial X_{pq}}{\partial M_K}=\sum_\alpha\omega(\alpha)\left[\sum_i h_K^{pi}<\alpha|E_{qi}|\alpha>\right] \qquad (27)$$

Once all the derivatives are calculated, they can be combined with the Lagrange multipliers to compute the hyperfine coupling tensors using Eq.(23):

$$\frac{dL(M,\lambda_{opt},\mu_{opt})}{dM_K}\bigg|_{M=0}=\left[\left(\sum_{\alpha\beta}D_\alpha D_\beta\frac{\partial(H_{eff})_{\alpha\beta}}{\partial M_K}/\sum_\alpha D_\alpha^2\right)+\sum_\alpha\sum_A\mu_{CASCI}^{A\alpha}\sum_B<A|H_K|B>C_B(\alpha)\right.$$

$$\left.+\sum_{p>q\in 0}\mu_{CASMO}^{pq}\left\{\sum_\alpha\omega(\alpha)\left[\sum_{pi}h_K^{pi}<\alpha|E_{qi}|\alpha>-\sum_{qi}h_K^{qi}<\alpha|E_{pi}|\alpha>\right]\right\}+\sum_{p\ge q\in D}\mu_{CASMO}^{pq}h_K^{pq}\right]_{M=0}$$

where $\dfrac{\partial (H_{\it eff})_{\alpha\beta}}{\partial M_K}$ is given by Eq.(25), and $\mu_{CASCI}^{A\alpha}$ and μ_{CASMO}^{pq} are determined by solving Eq.(41) and Eq.(43) in ref. [6].

7. Concluding remarks

Analytic calculation of the hyperfine coupling tensors for MCQDPT theory developed in this chapter relies on the evaluation of the Lagrange multipliers using the formalism derived in ref. [6]. Once these multipliers are calculated, the evaluation of the magnetic derivatives presents a relatively straightforward task. The derivation presented in this chapter includes all the limitations placed on the evaluation of the Lagrange multipliers in ref. [6]. However, these limitations are not related to the evaluation of magnetic derivatives in particular. One important limitation put on the derivation here and in ref. [6] is the use of the same set of reference functions for both the MCSCF and MCQDPT calculations. It is often advantageous to use a different reference in the MCQDPT calculation. For example, using orbitals from a singlet MCSCF calculation for triplet MCQDPT states often simplifies calculations of excited states. Equations for the Lagrange multipliers obtained without this restriction on the set of reference functions can be found in ref. [7]. Using these multipliers to evaluate the hyperfine coupling tensors according to the procedure derived here does not require any modifications.

References

1. T.Helgaker, M.Jaszunski, K.Ruud, Chem. Rev. 99, 293 (1999)

2. J.Kowalewski, Prog.NMR Spectrosc. 11, 1 (1977)

3. J.Kowalewski, A.Laaksonen, In Theoretical Models of Chemical Bonding, Part 3; Z.B.Maksic, Ed.; Springer-Verlag: Berlin 1991; p 387

4. M.W.Schmidt, M.S.Gordon, Ann. Rev. Phys. Chem. 49, 233 (1998)

5. O.Vahtras, H.Ågren, P.Jørgensen, H.J.Jensen, S.Padkjær, T.Helgaker, J.Chem.Phys. **9 6**, 6120 (1992)

6. H.Nakano, K.Hirao, M.S.Gordon, J.Chem.Phys. **1 0 8**, 5660 (1998)

7. H.Nakano, N.Otsuka, K.Hirao, In Recent Advances in Multireference Methods; K.Hirao, Ed.; World Scientific: Singapore, 1999; p 1 3 1

8. T.Helgaker, P.Jørgensen, In Methods in Computational Molecular Physics; S.Wilson, G.H.F.Diercksen, Eds.; Plenum Press: New York, 1992; p 3 5 3

9. T.Helgaker, P.Jørgensen, Theor.Chim. Acta, **7 5**, 111 (1989)

10. H.Nakano, J.Chem.Phys. **9 9**, 7983 (1993)

11. H.Nakano, Chem.Phys.Lett. **2 0 7**, 3 7 2 (1993)

CHAPTER 5: THE POTENTIAL ENERGY SURFACES FOR AlO₂ USING MULTI-REFERENCE WAVE FUNCTIONS

Michael V. Pak and Mark S. Gordon

Abstract

We report a systematic multi-configurational study of several low lying states of AlO_2 in a wide region of the coordinate space, in order to provide additional insight into the electronic structure of the AlO_2 molecule. This work attempts to resolve the question of the global minimum energy structure for the AlO_2 molecule. A symmetry breaking observed in the vicinity of the linear geometry at the multi-configurational self-consistent field (CASSCF) level of theory is shown to be due to insufficient accounting of dynamic correlation, since it does not appear in multi-reference configuration interaction (MRCI) or multi-reference perturbation theory calculations (MCQDPT).

1. Introduction

It has been suggested, based primarily on thermodynamic considerations, that adding a small number (~ 5% by weight) of Al atoms to solid hydrogen to be used as a rocket propellant can considerably increase the fuel efficiency. However, the possibility of a practical implementation of this idea depends on various details of the reaction of Al with O_2, thus providing a strong impetus for theoretical studies of this reaction. It is quite

reasonable to expect that AlO_2 plays a key role in the $Al + O_2$ reaction. Several studies have suggested that AlO_2 is one of the major products observed in a reaction of evaporated Al atoms with O_2 in a cryogenic matrix [1,2]. A complete analysis of the structure and mechanism of the formation of AlO_2 is an important and necessary step toward a detailed understanding of the process of Al combustion.

In the present work we attempt to determine definitively the global minimum energy structure for the AlO_2 molecule. There is a large amount of experimental data available from numerous matrix isolation experiments [1,3-5] and at least one gas-phase study [6] of the $Al + O_2$ reaction. However, characterization of the structure of the products of this reaction relies substantially on the analysis of the infrared (IR) spectra, and definitive assignments of frequencies are not always possible without the necessary complementary information from theoretical studies. The available experimental data are insufficient to firmly establish the structure of the AlO_2 molecule, and must therefore be complemented by results of high accuracy *ab initio* calculations.

The conclusion of the experimental works [1,3-6], that the AlO_2 molecule exists as two different isomers - one linear and one cyclic, seems to be in good agreement with the results of previous theoretical studies [2,7-8,12]. Calculations by Rubio et al. [7,8] predicted a C_{2v} cyclic structure, with an O-Al-O angle of about 70°, to be a true minimum on the restricted Hartree-Fock (RHF) potential energy surface (PES). This study did not locate a stable C_S structure, even though such a structure was predicted in the experimental work of Sonchik, Andrews and Carlson [4]. An unrestricted Hartree-Fock (UHF) calculation predicted one imaginary frequency for the C_{2v} structure. This was attributed to a Hartree-Fock instability problem [9-11].

An extensive theoretical study by Nemukhin and Almlöf [12] employed large basis sets and the CASSCF [13,14,15] approximation. The

study supported the results of Rubio et al. [8], predicting the cyclic form of AlO_2 to be an energy minimum on the A_2 PES, with an O-Al-O angle of 41.8°. However, another stationary point, corresponding to a linear $D_{\infty h}$ structure, not investigated at all in [8], was found to have even lower energy than the cyclic structure. It was not clear if this structure is a true minimum on the PES, since there was an apparent symmetry breaking in the CASSCF wave function. This symmetry breaking was attributed to the omission of the O 2s orbitals from the CASSCF active space. Since all other frequencies calculated for the linear and the cyclic isomers of AlO_2 seemed to be in good agreement with the results of spectroscopic studies, it was concluded that no further studies of the ground state PES were necessary to explain the existing experimental data. The energy difference between the two structures was found to be only about 6 kcal/mol, thus leaving the final conclusion regarding the ground state structure of AlO_2 unresolved.

A relatively high lying structure having C_S symmetry was found by Marshall et al. [16]. This study also reported an instability in the $D_{\infty h}$ wave function, resulting in symmetry breaking distortions from $D_{\infty h}$ to $C_{\infty v}$. However, the UHF level of theory employed in this work may not be reliable [7,8,12].

The cyclic structure was studied again by Archibong, Leszczynski and Sullivan [2], employing larger basis sets and a more complete treatment of electron correlation. Using the coupled cluster method including all single and double excitations with the effect of connected triple excitations included perturbatively (CCSD(T)) reproduces the findings of Nemukhin and Almlöf regarding this C_{2v} structure, except for some minor details. Linear AlO_2 was not studied by these authors.

The brief review of previous theoretical studies given above demonstrates that the identity of the ground state of AlO_2 is still unresolved. In particular, the problem of symmetry breaking remains an

open question. Some of the vibrational frequencies predicted in the most accurate of the above reports [2,12] disagree with experimentally observed frequencies by up to 100 cm^{-1}. In this work, we report a systematic multi-configurational study of all low lying states of both C_{2v} and C_S symmetry in a wide region of the coordinate space, including the vicinity of linear $C_{\infty v}$ and $D_{\infty h}$ geometries, in order to provide additional insight into the electronic structure of the AlO_2 molecule.

2. Methods

All calculations were performed with the GAMESS [17] and MOLPRO [18,19] programs, using the 6-311G* basis set [20] with a total of 65 basis functions. Geometry optimizations were carried out at the MCSCF level, with a CASSCF active space including all valence orbitals of Al and O atoms (15 electrons in 12 orbitals). The MCQDPT2 [21,22] and MRCI [18,19] calculations employed the same active space as the MCSCF calculations. All electronic states discussed here are doublet states.

3. Results and discussion

An overview of the MCSCF PES for the C_{2v} A_1, A_2 and B_1 states and the C_S A' and A" states is given in Figure 1. The O-Al-O angle, chosen as a reaction coordinate, was varied from about 40 to 180 degrees, and the Al-O bond lengths were optimized for each fixed angle. Thus, the curves presented in Figure 1 may be thought of as reaction paths for the isomerisation reaction leading from cyclic to linear AlO_2.

The dominant MCSCF configuration near the cyclic A_2 minimum can be written as $(6a_1)^2(7a_1)^2(4b_1)^2(2b_2)^2(8a_1)^2(1a_2)^1$. Here, $4b_1$ and $1a_2$ are the two π^* O-O orbitals, and $8a_1$ is almost entirely the 3s orbital of Al. There are three orbitals in the MCSCF active space which have the character of the 3p Al orbitals; all of them are vacant in the leading configuration. These three

orbitals remain vacant everywhere on all PES's studied, including the vicinity of the linear geometry. The leading MCSCF configuration near the linear geometry is $(6a_1)^2(7a_1)^2(4b_1)^2(2b_2)^2(5b_1)^2(1a_2)^1$, with almost an equal contribution from the $(6a_1)^2(7a_1)^1(4b_1)^2(2b_2)^2(8a_1)^1(5b_1)^2(1a_2)^1$ configuration. The $5b_1$ orbital here has a σ^* O-O character.

For angles smaller than about $60°$ the C_S states are identical to the corresponding C_{2v} states. For these small angles, the lowest energy minimum is on the A_2 PES, with both A_1 and B_1 minima lying higher. Our results for the geometric parameters at all C_{2v} minima agree well with the previous MCSCF study [12] (see Table 1).

For angles larger than $80°$ a symmetry breaking occurs in the MCSCF wave function. As a result, the two Al-O distances become unequal, and optimized structures have C_S symmetry. Constrained geometry optimizations of course provide optimized structures with C_{2v} symmetry, but they appear to be unstable with respect to the asymmetric stretch mode and thus are not true minima on the MCSCF PES. It was suggested [12] that this symmetry breaking might be caused by omitting the 2s oxygen orbitals from the active space in the CASSCF wave function. In this work the active space included the 2s O orbitals, so this is clearly not the origin of the apparent symmetry breaking.

It is worth emphasizing that, unlike most usual cases of symmetry breaking (e.g. doublet instability) [23], the C_S symmetry structures are energetically favored over the C_{2v} structures not only in the immediate vicinity of the linear geometry, but in a large region of coordinate space.

The MCSCF wave function does not change smoothly between C_{2v} and C_S nuclear configurations, and the resulting PES has an artificial cusp at the C_{2v} geometry. For example, for a fixed bond angle of $120°$, changing one of the Al-O distances from its C_{2v} optimized value of 1.7002Å to 1.7001Å, which formally lowers the symmetry of the molecule to C_S, results in the energy being lowered by 2.6 kcal/mol. A subsequent geometry optimization

in C_S symmetry lowers the energy by only 1.8 kcal/mol, although the bond distances change substantially (to 1.7561 Å and 1.6452 Å). An analysis of the MCSCF wave function shows that the energy lowering does not involve any significant changes in the optimized orbitals; however, the CI coefficients change considerably in a very small region of coordinate space around the C_{2v} geometry.

At 180° (Fig.1) the A' and A" states become two degenerate Π states in $C_{\infty v}$ symmetry. This appears to be the global minimum on the CASSCF doublet PES of AlO_2.

Now, consider the effect of dynamic correlation on the AlO_2 potential energy curves. Figure 2 shows single point MCQDPT2 energies calculated at the MCSCF optimized geometries. At this level of theory, C_{2v} structures have lower energy than the corresponding C_S states at all angles. Apparently, dynamic correlation is more important for symmetric geometries than for symmetry broken ones. This is illustrated by the MCSCF, MCQDPT2 and MRCI energies given in Table 2 for the $D_{\infty h}$ Π_g states (corresponding to the C_{2v} A_2 and B_1 states for nonlinear structures) and the $C_{\infty v}$ Π states (corresponding to the C_S A' and A" states).

The MCQDPT2 and MRCI results clearly demonstrate that the symmetry breaking observed at MCSCF level of theory is not physical and is due to insufficient accounting for dynamic correlation. So, the MCSCF treatment of AlO_2 is not sufficient.

The MCSCF energy difference between the cyclic and the linear structures is only 0.0062 E_h. This makes these structures almost isoenergetic [12]. At the MCQDPT2 level the difference is almost 10 times larger (.05 E_h), thus firmly establishing the Π_g state of the linear structure as the global energy minimum of AlO_2.

4. Conclusions

The doublet potential energy surfaces of AlO_2 have been studied in a wide region of the coordinate space between the linear and the cyclic structures, using the CASSCF, MCQDPT and MRCI methods. It is shown that an insufficient treatment of dynamic correlation at the CASSCF level of theory leads to a symmetry breaking in the vicinity of the linear geometry. This symmetry breaking is not observed in MCQDPT and MRCI calculations.

At the MCQDPT/6-311G(d) level, linear AlO_2 is about 31 kcal/mol lower than the cyclic structure. The barrier leading from the cyclic to the linear AlO_2 at this level of theory is approximately 60 kcal/mol. Using the same level of theory with the larger cc-pvtz basis set results in approximately the same energy difference between the two isomers: 33 kcal/mol favoring the linear structure. The large energy difference between the two main isomers of the AlO_2 molecule at the MCQDPT level disagrees with the results of the current and previous MCSCF studies [12] which predict the two structures to have similar energies. The linear structure appears to be well established as the global energy minimum for the AlO_2 molecule.

References

1. L.Andrews, T.R.Burkholder, J.T.Yustein, J.Phys.Chem. **96**, 10182 (1992)

2. E.F.Archibong, J.Leszczynski, R.Sullivan, J.Mol.Struct. **425**, 123 (1998)

3. L.V.Serebrennikov, S.B.Osin, A.A.Maltsev, J. Mol. Struct. **81**, 25 (1982)

4. S.M.Sonchik, L.Andrews, K.D.Carlson, J.Phys.Chem. **87**, 2004 (1983)

5. I.L.Rozhanskii, G.V.Chertikhin, L.V.Serebrennikov, V.F.Shevel'kov, Russ.J.Phys.Chem. **62**, 1215 (1988)

6. S.R.Desai, H.Wu, L Wang, Int.J.Mass.Spectrom.Ion.Proc. **159**, 75 (1996)

7. J.Masip, A.Clotet, J.M.Ricart, F. Illas, J.Rubio, Chem.Phys.Lett. **144**, 373 (1988)

8. J.Rubio, J.M.Ricart, F. Illas, J.Comput.Chem. **9** , 836 (1988)

9. J.Paldus, A.Veillard, Mol.Phys. **35**, 445 (1978)

10. O.Kikuchi, Chem.Phys.Lett. **72**, 487 (1980)

11. E.R.Davidson, W.T.J.Borden, J.Phys.Chem. **87**, 4783 (1983)

12. A.V.Nemukhin, J. Almlöf, J.Mol.Struct. **253**, 101 (1992)

13. B.O.Roos, P.R.Taylor, P.E.M.Siegbahn, Chem.Phys. **48**, 157 (1980)

14. B.O.Roos, Adv.Chem.Phys., **69**, 399 (1987)

15. K.Ruedenberg, M.W.Schmidt, M.M.Gilbert and S.T.Ebert, Chem.Phys. **71**, 41, 51, 65 (1982)

16. P.Marshall, P.B.O'Connor, W.Chan, P.V.Kristof, J.D.Goddard, Gas-Phase Met. React. 147 (1992)

17. M.W.Schmidt, K.K.Baldridge, J.A.Boatz, S.T.Elbert, M.S.Gordon, J.H.Jensen, S.Koseki, N.Matsunaga, K.A.Nguyen, S.J.Su, T.L.Windus, M.Dupuis, J.A.Montgomery, J.Comp.Chem. **14**, 1347 (1993)

18. H.-J.Werner and P.J.Knowles, J.Chem.Phys. **89**, 5803 (1988)

19. P.J.Knowles and H.-J.Werner, Chem.Phys.Lett. **145**, 514 (1988)

20. R.Krishnan, J.S.Binkley, R.Seeger, J.A.Pople, J.Chem.Phys. **72**, 650 (1980)

21. H.Nakano, J.Chem.Phys. **99**, 7983 (1993)

22. K.Hirao, Chem.Phys.Lett. **190**, 374 (1992)

23. L.Engelbrecht, B.Liu, J.Chem.Phys. **78**, 3097 (1983)

Table 1. Molecular parameters for symmetric AlO_2 structures.

Ref.#	Method	linear ($D_{\infty h}$)	cyclic (C_{2v})	
		d_{AlO} (Å)	d_{AlO} (Å)	α_{OAlO} (°)
[8]	CIPSI	1.794	1.994	69.9
[13]	UHF	1.655	1.930	39.5
[12]	MCSCF	1.670	1.930	41.8
[2]	CCSD(T)	-	1.940	40.9
This work	MCSCF	1.675	1.956	41.1
This work	MCQDPT2	1.676	1.952	41.1

Table 2. MCSCF, MCQDPT and MRCI energies for the symmetric ($D_{\infty h}$) and symmetry-broken ($C_{\infty v}$) linear AlO_2 (a.u.) (6-31G* basis set)

	$D_{\infty h}$	$C_{\infty v}$
MCSCF	-391.69455	-391.71224
SA-MCSCF [a]	-391.69267	-391.71059
MCQDPT	-391.97286	-391.96180
MRCI	-391.96105	-391.95985

[a] State averaged MCSCF, averaging over two degenerate Π states
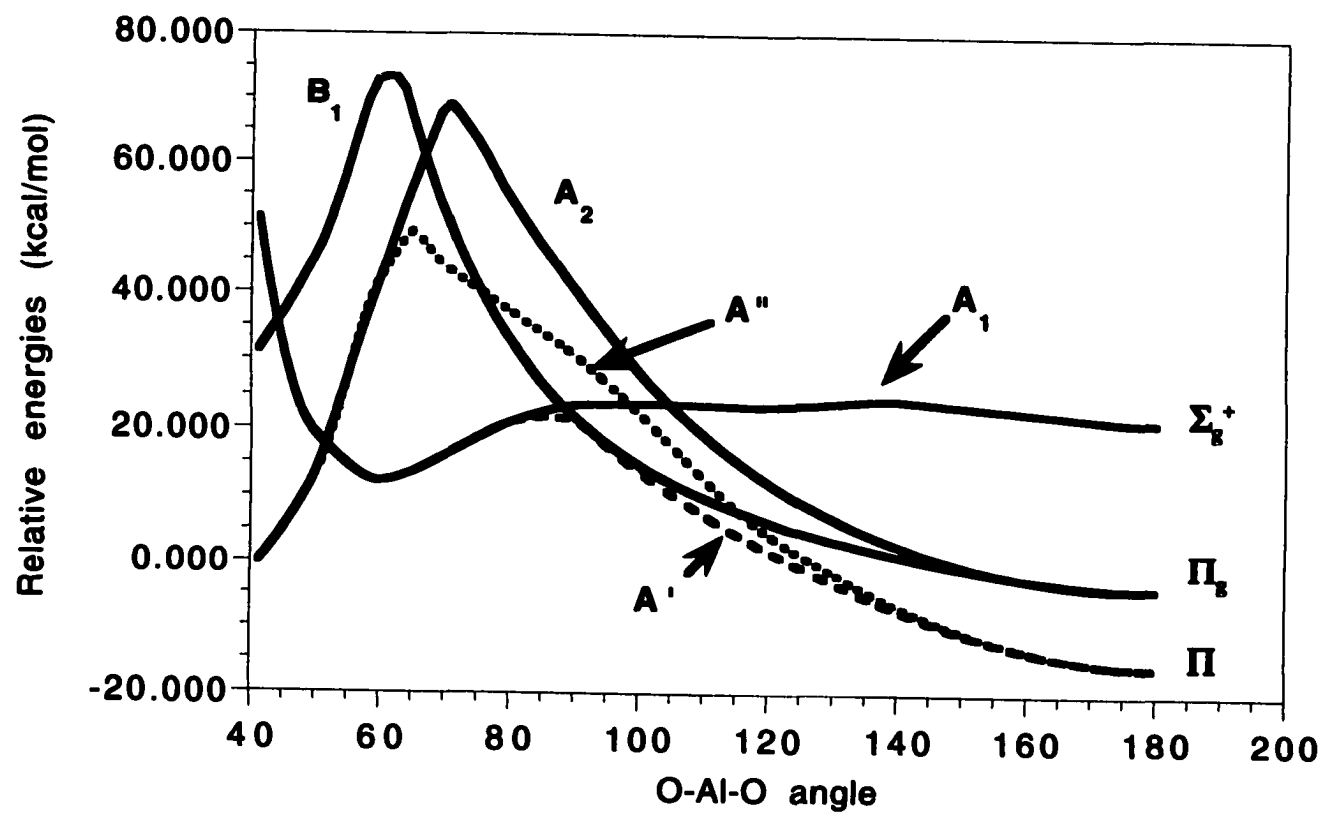
Figure 1. MCSCF/6-311G(d) reaction paths for the $^2A_1$, $^2A_2$, $^2B_1$, $^2A'$ and $^2A''$ states.
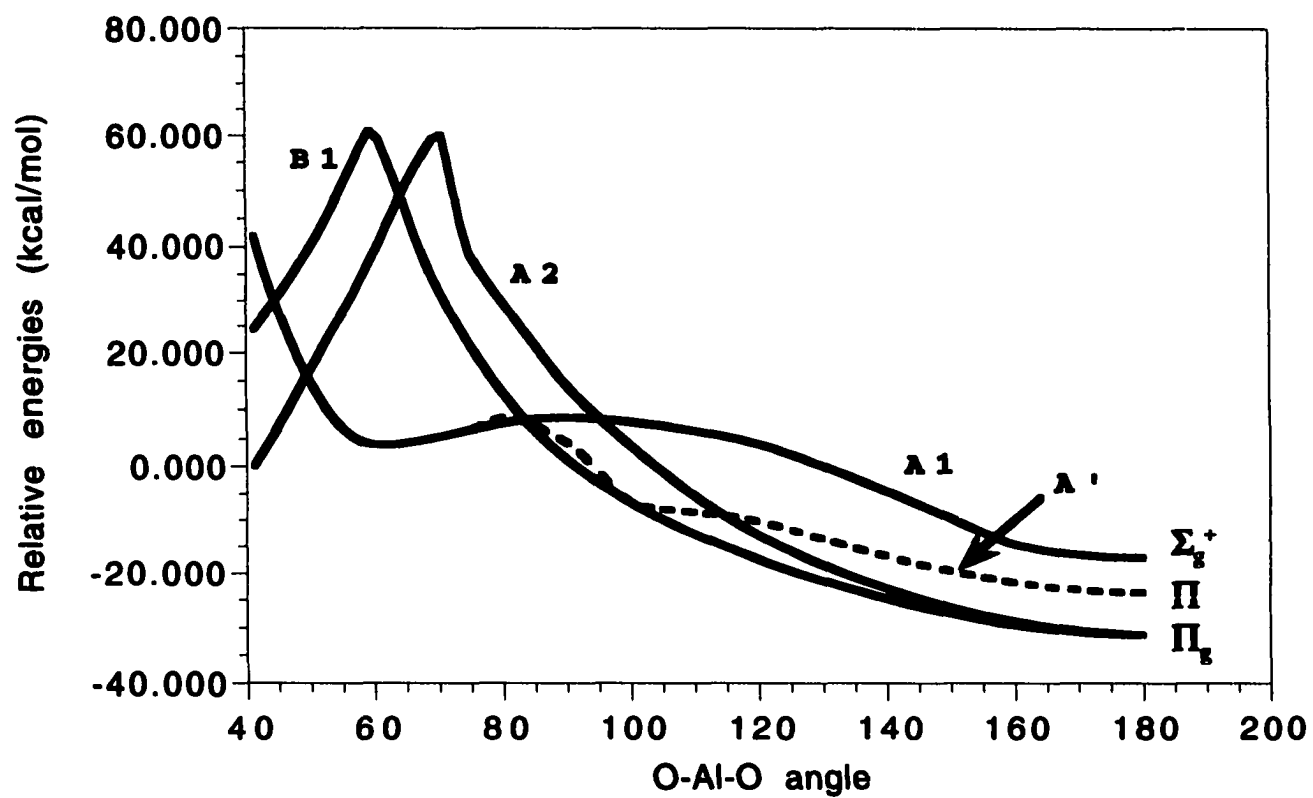
Figure 2. MCQDPT2/6-311G(d) reaction paths for the $^2A_1$, $^2A_2$, $^2B_1$, and $^2A'$ states.

CHAPTER 6: POTENTIAL ENERGY SURFACES FOR THE Al + O$_2$ REACTION

A paper to be submitted for publication to

Journal of Chemical Physics

Michael V. Pak and Mark S. Gordon

Abstract

We present a systematic multi-configurational study of the first two doublet potential energy surfaces of atomic aluminum with molecular oxygen. The most likely products, AlO and AlO$_2$, are expected to figure prominently in subsequent reactions to form Al$_2$O$_3$. The main reaction pathways on both surfaces invariably lead to the formation of cyclic AlO$_2$, possibly followed by isomerization to the lower energy linear AlO$_2$ isomer. A reaction path leading from Al + O$_2$ directly to AlO + O was not located. However, both AlO$_2$ isomers can dissociate to AlO + O with no barrier beyond endothermicity. There is also no barrier for the reaction of AlO$_2$ with AlO to form Al$_2$O$_3$, and this reaction is highly exothermic.

I. Introduction

The reaction of Al atoms with oxygen is of considerable interest in view of the potential use of aluminum doped solid hydrogen as a rocket propellant. It has been predicted that solid H_2 doped with 5% aluminum atoms would be 80% more dense than liquid H_2, and would therefore give a 10% specific impulse increase, corresponding to a 200% payload increase [1]. However, this prediction is based on the assumption that all of the aluminum present in the system is oxidized into Al_2O_3. In fact, using pure solid H_2 is preferable over Al-doped H_2, if any other Al oxides are generated in substantial quantities as final products of combustion, since the exothermicities of all other aluminum oxides are much smaller than that of Al_2O_3[2]. Therefore, it is important to develop a quantitative understanding of the energetics of aluminum combustion.

In this paper, we report a systematic study of the potential energy surfaces for possible mechanisms of the reactions of Al with O_2, since the most likely products, AlO and AlO_2, are expected to figure prominently in subsequent reactions to form Al_2O_3.

Most of the theoretical and experimental works on aluminum combustion available in the literature [3-5] deal with the combustion of metallic aluminum. While some thermodynamic data provided in those studies are also relevant for the reaction of isolated Al atoms with oxygen, there are some important differences between these two processes which make most of the conclusions made regarding the combustion of solid Al inapplicable to the present study. For example, in a very extensive theoretical study of energetics of aluminum combustion by Politzer, Lane and Grice [4] it is implied that there is a large number of molecules containing carbon, nitrogen and other elements present in the system. This is certainly true in the case of combustion of metallic aluminum, usually added to organic propellants. However, the major route to Al_2O_3 in such

systems is believed to be the CO_2 oxidation of aluminum, and this is not directly relevant to the combustion of Al atoms trapped in solid H_2 matrix.

Another important distinction is the number of Al atoms involved in the first elementary steps of the combustion mechanism. Since the present study addresses a reaction of isolated Al atoms very sparsely dispersed in a solid hydrogen matrix, with less than 5% of Al present [1,6], elementary steps involving more than one Al atom are unlikely. For example, the possibility of formation of Al_2O in a reaction of two Al atoms with either O_2 or O, which could be important in the combustion of solid Al particles, is not considered.

There are a number of experimental and theoretical studies of various molecular species present in the $Al + O_2$ system available in the literature [3-5,7-16]. Most of these works focus on the electronic structure and properties of Al oxides and not on the reaction mechanisms leading to their formation. An exception is the theoretical study by Marshall et al. [4], that provides some information about the thermochemistry and kinetics of the $Al + O_2$ reaction. However, the unrestricted Hartree-Fock (UHF) formalism used in that work for AlO and AlO_2 (two of the key products) may be suspect due to serious spin contamination. For the two key structures in the $Al + O_2$ reaction, AlO and AlO_2, the UHF wave functions showed instabilities, and the authors concluded that more flexible wave functions were needed to describe these molecules. Since a broad section of the potential energy surfaces for several electronic states are of interest, the multi-reference wave functions used in the present work seem more appropriate.

The goal of this paper is to present a systematic and consistent study of the potential energy surfaces for the $Al + O_2$ system, using multi-configurational wave functions and dynamic correlation corrections for all stationary states on these surfaces. Based on the following analysis of the

low-lying PES's for this system, the most probable mechanisms leading to the formation of Al_2O_3 are proposed.

II. Methods

All calculations reported in the present work have been carried out with the GAMESS [17] and MOLPRO [18,19] programs. The PES's were studied at the MCSCF level with the complete active space SCF (CASSCF) or the fully optimized reaction space (FORS) [20-21] active spaces varying in size from including all valence electrons to including only the electrons involved in chemical changes. The full valence active space was used in MCSCF calculations of all minima on the potential energy surfaces. The active spaces used in the MCSCF study of reaction mechanisms will be described later in this paper.

The energies of the minima and the transition states were recalculated at the CCSD(T), second order multi-reference perturbation theory (MRMP2 [22-23]) and multi-reference configuration interaction (MRCI [18-19]) levels of theory. The MRCI wave function included all single and double excitations from the FORS reference space into the virtual space, referred to as MR(SD)-CI [18,19]. Dynamic reaction path (DRP) [24-25] calculations were used to examine the most probable reaction channels on the PES's. To verify the basis set convergence, most of the calculations, including geometry optimizations of all stationary points on the PES's, were performed subsequently with 6-311G* [26], aug-cc-pvTZ and aug-cc-pvQZ [27] basis sets.

III. Results and discussion

A. AlO₂ and AlO.

The reaction of a single Al atom with an oxygen molecule can result in the formation of either AlO_2, or AlO and an oxygen atom:

$$Al + O_2 \rightarrow AlO_2 \qquad (1)$$

$$Al + O_2 \rightarrow AlO + O \qquad (2)$$

In order to predict the most probable outcome of this reaction, it is important to understand the electronic structure of all the species involved. First, consider aluminum dioxide, AlO_2. The global minimum energy structure of AlO_2 has been a subject of extensive study [11-14,28], with two potential candidates being the linear $OAlO$ and the cyclic AlO_2 isomers. The lowest energy PES for C_{2v} AlO_2 is the $^2A_2$ state, with the $^2A_1$ state being higher in energy for both isomers. The $^2A_2$ state corresponds to $^2\Pi_g$ and $^2A_1$ to $^2\Sigma^+_g$ in $D_{\infty h}$ symmetry. It was shown earlier [28] that at the MRMP2/cc-pvTZ level, linear AlO_2 lies about 33 kcal/mol lower than the cyclic structure. The barrier leading from the cyclic to the linear AlO_2 is approximately 60 kcal/mol at this level of theory.

In this work, the energy splitting between the $^2A_2$ and $^2A_1$ states of AlO_2 has been re-evaluated for both the linear and the cyclic structure. The results are presented in Table 1, together with the results of Archibong et al. [7] for the cyclic structure. No similar data are available in the literature for the linear structure, probably because this species presents additional difficulty for theoretical study due to a symmetry breaking in the MCSCF wave function (see discussion in [28]). The $^2A_2$ - $^2A_1$ energy difference is relatively small for the cyclic structure, converging to a value of approximately 4.5 kcal/mol. One clearly needs a good basis set and a well-correlated wave function to achieve this result. For linear AlO_2, the energy difference is much larger. The dynamical correlation effects are significant at this geometry, with MCSCF overestimating the splitting by more than 10 kcal/mol compared to the MRCI result for the same basis set.

At the CCSD(T)/aug-cc-pvQZ level, the $^2A_2$ state of cyclic AlO_2 is about 68 kcal/mol lower in energy than the reactants $Al + O_2$ (63.5 kcal/mol for the $^2A_1$ state). The energy of the linear structure on the $^2A_2$ potential energy surface is almost 30 kcal/mol lower; however, there is a 60 kcal/mol barrier (at the MRMP2/aug-cc-pvTZ level) between the cyclic and the linear isomers. For the $^2A_1$ state both the energy difference between the cyclic and the linear structures and the barrier between those isomers are much smaller than the corresponding values for the $^2A_2$ PES. At the MRMP2/aug-cc-pvTZ level, on the $^2A_1$ surface the linear isomer is only 18 kcal/mol lower in energy than cyclic AlO_2, and the barrier between the isomers is smaller than 10 kcal/mol.

For AlO the $^2\Sigma^+$ state is predicted to be lower in energy than the doubly degenerate $^2\Pi_i$ state. The energy splitting between these two states, calculated at different levels of theory, is given in Table 2. The estimated best value (MRCI/aug-cc-pvQZ) of 15.6 kcal/mol is in very good agreement with the experimental value of 15.0 ± 0.3 kcal/mol [2,29]. The overall exothermicity of reaction (2) for the lowest energy electronic state ($^2\Sigma^+$) of AlO, calculated at the CCSD(T)/aug-cc-pvQZ level of theory is estimated at 3.1 kcal/mol, very close to the experimental value of about 3.2 kcal/mol [2,30]. The formation of AlO in the $^2\Pi_i$ state is 12 kcal/mol endothermic (at the MRCI/aug-cc-pvQZ level).

It appears that at least thermodynamically the formation of AlO_2 is greatly favored over the formation of AlO + O. Even if we consider the higher energy cyclic AlO_2, the energy gain in reaction (1) is almost 65 kcal/mol greater than that in reaction (2). The products of reaction (2) are almost isoenergetic with the reactants, while the formation of AlO_2 is highly exothermic.

B. Reaction mechanisms. To predict the kinetics of these reactions, detailed knowledge of the PES for the Al + O_2 system is required. The next goal is to find the reaction paths and transition states for both reactions (1) and (2), as well as a reaction path for possible dissociation of AlO_2 into AlO + O - another possible source of AlO in the system:

$$AlO_2 \rightarrow AlO + O \qquad (3).$$
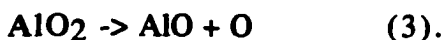
To build a map of the potential energy surface for the Al + O_2 reaction, consider an Al atom approaching the oxygen molecule from different directions (Figure 1a). Ideally, it would be desirous to use a full valence active space MCSCF wave function to describe this process. However, if all valence electrons of Al and O_2 are included in the active space, the MCSCF optimization converges to an intruder state at all geometries for which the Al-O distance is larger than about 2.5Å.

A logical active space is composed of those electrons and orbitals that are involved in the chemical changes due to the interaction of Al and O_2. The formation of the $^2A_2$ state of AlO_2 can be qualitatively described as electron transfer from the singly occupied p orbital of Al into the in-plane π^* orbital of the O_2 molecule. The out-of-plane π^* orbital remains singly occupied. The $^2A_1$ state of AlO_2 arises from the transfer of two electrons from Al - one p and one s - into the two π^* orbitals of O_2. Therefore, a n active space including the two π^* orbitals of O_2 plus the 3s and one of the 3p orbitals of Al should be adequate for the description of orbital changes in this reaction. In fact, the results obtained with the active space just described are in good agreement with results produced with various larger active spaces, up to the full valence active space, when the latter is not plagued by intruder states. The orbital changes in reaction (2) require all of the O_2 valence orbitals to be present in the active space, as well as the 3s

and at least one of the 3p Al orbitals. The inclusion of the remaining two $3p$ orbitals of Al does not appear to be necessary.

Therefore, to study reaction (1), an active space composed of the two π^* orbitals of O_2 and the 3s and one of the 3p orbitals of the Al atom was used. The $3p_x$ orbital of Al was used for the $^2A_2$ PES, and the $3p_y$ orbital - for the $^2A_1$ state. The active space used for reaction (2) includes all valence orbitals of the two oxygen atoms and the 3s and one of the 3p orbitals of Al. Expanding the active space used for reaction (1) to include all valence orbitals of oxygen does not have any noticeable effect on the results, justifying the use of a smaller active space for this reaction.

The MCSCF PES for the system shown in Figure 1a was investigated for a large variety of distances R and angles α. The $^2A_1$ state of the Al + O_2 system becomes A' in C_s symmetry, and the $^2A_2$ state becomes A". The A' and A" potential energy surfaces were investigated using a series of constrained optimizations, with the O-O distance optimized for different fixed values of distance R and angle α. It appears that on both the A' and A" PES's there are no minima that have C_s symmetry. A geometry optimization beginning at any C_s geometry always results in a C_{2v} symmetric structure. There also appears to be no first-order saddle point with C_s symmetry. Apparently, the interaction of an Al atom approaching the O_2 molecule from different directions invariably leads to the formation of cyclic AlO_2, on both the A' and A" PES's. On the A" surface, there seems to be no barrier for this reaction in C_s symmetry; for the C_{2v} ($^2A_2$) approach there is a very small barrier of about 4 kcal/mol at the MRMP2/6-311G* level of theory. The $^2A_2$ transition state has $R_{AlO}=2.87$Å and $R_{OO}=1.16$Å. At the MCSCF/6-311G* level, the imaginary frequency is 176.9 cm^{-1}. Following the intrinsic reaction coordinate (IRC) along the normal mode associated with this

frequency leads to the cyclic AlO_2 in one direction and free $Al + O_2$ in the opposite direction.

The structure of the A' PES is somewhat different from that of the A" surface. The barrier for the C_{2v} ($^2A_1$) approach is about 22 kcal/mol at the MRMP2/6-311G* level.

To locate a reaction path leading from $Al + O_2$ directly to $AlO + O$ (reaction (2)), consider the $C_{\infty v}$ arrangement shown in Figure 1b, with Al aligned in a collinear arrangement with the O_2 molecule. Constrained geometry optimizations for various fixed values of one AlO distance produce a stationary point in $C_{\infty v}$ symmetry. This stationary point has two imaginary frequencies that correspond to the degenerate linear bend. Therefore, it appears that there is no C_s or $C_{\infty v}$ reaction path that leads to $AlO + O$. This is consistent with the results of Politzer et al [5], who were unable to find a doublet transition state for reaction (2) anywhere on the PES (they did not consider reaction (1)).

To further analyze the lowest energy PES for the $Al + O_2$ system, a series of MCSCF dynamic reaction path (DRP) calculations were performed, in which an Al atom having some initial kinetic energy was directed towards the O_2 molecule with different angles α. Depending on the angle of attack and the initial kinetic energy, the DRP calculations produced only two types of trajectories. For relatively small initial energies (less than 15 kcal/mol) the resulting trajectory almost invariably led to the formation of cyclic AlO_2. For initial kinetic energies greater that 15 kcal/mol, most trajectories resulted in dissociation of the $Al-O_2$ complex back to $Al + O_2$ immediately after collision. No DRP trajectories leading to $AlO + O$ were observed.

The existence of a very high barrier for the cyclic-to-liner isomerization of AlO_2 provides a hint at a possible explanation for the

difficulty of locating a minimum energy path for reaction (2). Breaking the very strong O_2 bond results in a relatively high barrier on the reaction path, even if the final products of the reaction are considerably lower in energy. In the case of the $Al+O_2$ system, the formation of cyclic AlO_2 does not involve completely breaking the O-O bond (only the π bond), results in a large energy gain and has either a very small or zero barrier, depending on the angle of attack of the Al atom. The formation of AlO + O, on the other hand, involves breaking the O_2 bond, which implies a large barrier, and the exothermicity of this reaction is only about 3 kcal/mol. Therefore, it is reasonable to expect that the main reaction channel leading to AlO should go through the formation of AlO_2, followed by its dissociation to AlO + O.

The reaction paths for the dissociation of AlO_2 (reaction 3), starting from both the cyclic and the linear AlO_2 have also been investigated. At the MRMP2/6-311G* level of theory, the dissociation of both structures appears to have no barrier beyond the endothermicity, in agreement with Marshall et al. [4]. Depending on the initial state of the AlO_2 molecule, the dissociation results in either $^2\Sigma^+$ (from the $^2A_1$ state of AlO_2) or $^2\Pi_i$ (from the $^2A_2$ state) state of AlO. At the MRCI/aug-cc-pvQZ level of theory, the combined energy of O + AlO in the $^2\Pi_i$ state (resulting from dissociation of the $^2A_2$ state of AlO_2) is about 12 kcal/mol higher than the energy required to dissociate AlO_2 into Al + O_2. However, due to the 4 kcal/mol barrier for the Al + O_2 dissociation reaction, the activation energy for this reaction is only 8 kcal/mol lower than the energy required for the AlO + O dissociation.

The AlO_2 -> AlO + O dissociation from the $^2A_1$ state is thermodynamically more favorable than the AlO_2 -> Al + O_2 dissociation by 3 kcal/mol. However, the relatively high barrier is 85 kcal/mol (at the

MRMP2/6-311G* level) for the reaction $AlO_2 \rightarrow Al + O_2$ in the $^2A_1$ state, while the AlO + O dissociation requires only about 60 kcal/mol.

C. AlO_2 + AlO reactions. According to an extensive theoretical study of Archibong and St-Amant [31], the lowest energy isomer of Al_2O_3 is the triplet C_{2v} structure, shown in Figure 2. This structure is about 7 kcal/mol lower in energy than the linear isomer previously established as the lowest energy stationary point on the singlet PES [15,32]. The lowest energy triplet state of C_{2v} Al_2O_3 is $^3B_2$. The $^3B_1$ state is about 3.5 kcal/mol higher in energy, and the linear $^1\Sigma_g^+$ Al_2O_3 is another 3.5 kcal/mol higher than the $^3B_1$ state of C_{2v} Al_2O_3. In this work, the formation of both the singlet and the triplet structures has been investigated.

First, consider the triplet potential energy surface. In C_{2v} symmetry, the $^2\Sigma^+$ state becomes $^2A_1$, and the doubly degenerate $^2\Pi_i$ state corresponds to $^2B_1/^2B_2$. The $^3B_2$ state of C_{2v} Al_2O_3 can result from the reaction of $^2A_1$ AlO_2 with the $^2B_2$ state of AlO, or from the reaction of $^2A_2$ AlO_2 with the $^2B_1$ state of AlO. The $^3B_1$ state can be formed in the reaction of AlO in the $^2\Pi_i$ ($^2B_1/^2B_2$) state with either $^2A_1$ or $^2A_2$ states of AlO_2. It is not possible to form either one of the lowest energy triplet states of Al_2O_3 from the lowest energy doublet states of AlO_2 and the $^2\Sigma^+$ ($^2A_1$) state of AlO. There is no barrier (at the MRMP2 level of theory) for the reaction of cyclic AlO_2 in the $^2A_1$ state with the $^2B_1/^2B_2$ states of AlO, to form the $^3B_1/^3B_2$ states of Al_2O_3 respectively. On the other hand, the reaction of $^2A_2$ AlO_2 with AlO in one of the $^2\Pi_i$ states does not lead to the formation of the lowest energy minima on the triplet PES of Al_2O_3. The triplet $^3B_1/^3B_2$ potential energy surfaces resulting from this reaction do not appear to have a stationary

point around the C_{2v} structure of Al_2O_3. Our results indicate that the triplet Al_2O_3 isomers are formed in the reaction of $^2\Pi_i$ AlO with cyclic AlO_2 in the $^2A_1$ state, but not in the lower energy $^2A_2$ state.

On the singlet PES, the $^1\Sigma_g^+$ state of Al_2O_3 results from the reaction of linear AlO_2 in the $^2\Sigma_g^+$ state with the $^2\Sigma^+$ state of AlO. There is no barrier for this reaction at the MRMP level of theory. The reaction of $^2\Pi_i$ AlO with the $^2\Pi_g$ state of linear AlO_2 leads to the formation of higher energy states of Al_2O_3.

IV. Conclusions

A survey of the $^2A_2$ PES of the Al + O_2 system predicts that the most favorable reaction pathways lead to the formation of cyclic AlO_2. Once this isomer of AlO_2 is formed, it can proceed further to the linear isomer, which involves surmounting a very high barrier of about 60 kcal/mol, or dissociate to AlO + O without any barrier beyond the endothermicity of about 80 kcal/mol. The dissociation of linear AlO_2 in $^2\Pi_g$ state to AlO + O is more than 100 kcal/mol endothermic.

The general features of the $^2A_1$ PES are quite similar. The most important differences between the two surfaces are the much smaller barrier leading from cyclic to linear AlO_2 on the $^2A_1$ PES [28] and the more favorable dissociation to AlO + O on this surface. Both AlO_2 minima on the $^2A_1$ surface are higher in energy than the corresponding minima on the $^2A_2$ PES: at the MRCI/aug-cc-pvTZ level the difference is 4.6 kcal/mol for the cyclic structure and about 16 kcal/mol for the linear isomer.

The reaction paths to AlO + O appear to go through the dissociation of AlO_2. There is no barrier for such dissociation on both potential energy

surfaces. For the $^2A_1$ state of cyclic AlO_2 and the corresponding $^2\Sigma^+_g$ state of linear AlO_2 this reaction is energetically favored over dissociation to Al + O_2. The activation energy of the AlO + O dissociation of the $^2A_2$ state of AlO_2 is only 8 kcal/mol higher than the activation energy of the Al + O_2 dissociation.

The lowest energy triplet Al_2O_3 isomers can be formed in the reaction of $^2\Pi_i$ AlO with cyclic AlO_2 in the $^2A_1$ state, but not in the lower energy $^2A_2$ state. The linear Al_2O_3 isomer results from the reaction of linear AlO_2 in the $^2\Sigma^+_g$ state with the $^2\Sigma^+$ state of AlO. There is no barrier for either of these reactions.

Acknowledgements

References

1. J.A.Sheehy, Proc.HEDM Contr.Conf. 12 (2001)

2. M.W.Chase, C.A.Davies, J.R.Downey, D.J.Frurip, R.A.McDonald, A.N.Syverup, JANAF Thermochemical Tables, J.Phys.Chem. Ref.Data, 14 (Suppl. No 1) (1985)

3. T.Basset, E.Daniel, J.C.Loraud, Can.J.Chem.Eng. 75, 938 (1997)

4. P.Marshall, P.B.O'Connor, W.Chan, P.V.Kristof, J.D.Goddard, Gas Phase Met. React. 147 (1992)

5. P.Politzer, P.Lane, M.E.Grice, J.Phys.Chem. A 105, 7473 (2001)

6. M.E.Fajardo, M.E.DeRose, S.Tam, Proc.HEDM Contr.Conf. 26 (2001)

7. E.F.Archibong, J.Leszczynski, R.Sullivan, J.Mol.Struct. 425, 123 (1998)

8. L.V.Serebrennikov, S.B.Osin, A.A.Maltsev, J. Mol. Struct. **81**, 25 (1982)

9. S.M.Sonchik, L.Andrews, K.D.Carlson, J.Phys.Chem. **87**, 2004 (1983)

10. I.L.Rozhanskii, G.V.Chertikhin, L.V.Serebrennikov, V.F.Shevel'kov, Russ.J.Phys.Chem. **62**, 1215 (1988)

11. S.R.Desai, H.Wu, L Wang, Int.J.Mass.Spectrom.Ion.Proc. **159**, 75 (1996)

12. J.Masip, A.Clotet, J.M.Ricart, F.Illas, J.Rubio, Chem.Phys.Lett. **144**, 373 (1988)

13. J.Rubio, J.M.Ricart, F.Illas, J.Comput.Chem. **9**, 836 (1988)

14. A.V.Nemukhin, J. Almlöf, J.Mol.Struct. **253**, 101 (1992)

15. A.V.Nemukhin, F.Weinhold, J.Chem.Phys., **97**, 3420 (1992)

16. G.I.Pangilinan, T.P.Russel, JCP, 111, 445 (1999)

17. M.W.Schmidt, K.K.Baldridge, J.A.Boatz, S.T.Elbert, M.S.Gordon, J.H.Jensen, S.Koseki, N.Matsunaga, K.A.Nguyen, S.J.Su, T.L.Windus, M.Dupuis, J.A. Montgomery, J.Comp.Chem. **14**, 1347 (1993)

18. H.-J Werner and P.J.Knowles, J.Chem.Phys. **89**, 5803 (1988)

19. P.J.Knowles and H.-J Werner, Chem.Phys.Lett. **145**, 514 (1988)

20. B.O.Roos, P.R.Taylor, P.E.M.Siegbahn, Chem.Phys., **48**, 157 (1980)

21. K.Ruedenberg, M.W.Schmidt, M.M.Gilbert and S.T.Ebert, Chem.Phys., **71**, 41, 51, 65 (1982)

22. H.Nakano, J.Chem.Phys. **99**, 7983 (1993)

23. K.Hirao, Chem.Phys.Lett. **190**, 374 (1992)

24. J.J.P.Stewart, L.P.Davis, L.W.Burggraf, J.Comput.Chem. **8**, 1117 (1987)

25. T.Takata, T.Taketsugu, K.Hirao, M.S.Gordon, J.Chem.Phys. **109**, 4281 (1998)

26. R.Krishnan, J.S.Binkley, R.Seeger, J.A.Pople, J.Chem.Phys. **72**, 650 (1980)

27. D.E.Woon, T.H.Dunning,Jr., J. Chem. Phys. **98**, 1358 (1993).

28. M.V.Pak, M.S.Gordon, Chem.Phys.Lett. **344**, 236 (2001)

29. B.H.Lengsfield, B.Liu, J.Chem.Phys. **77**, 6083 (1982)

30. W.G.Mallard, P.J.Linstrom, Eds.; NIST Chemistry Webbook, NIST Standard reference Database No.69; NIST: Gaithersburg, MD, 1998

31. E.F.Archibong, A.St-Amant, J.Phys.Chem. **103**, 1109 (1999)

32. L.Andrews, T.R.Burkholder, J.T.Yustein, J.Phys.Chem. **96**, 10182 (1992)

Table 1. Energy splitting between the $^2A_2$ and $^2A_1$ states of cyclic AlO_2 ($^2A_2$ lower) and between the $^2\Pi_g$ and $^2\Sigma^+_g$ states of linear AlO_2 ($^2\Sigma^+_g$ lower) (kcal/mol).

| Method	cyclic (C_{2v})	linear ($D_{\infty h}$)
UHF/6-311G++(3df) [a]	13.9	-
MCSCF/6-311G* [b]	12.0	26.0
MCSCF/aug-cc-pvTZ [b]	8.8	26.6
MCSCF/aug-cc-pvQZ [b]	7.8	25.7
CCSD(T)/cc-pvTZ [b]	8.2	15.7
CCSD(T)/6-311G(2df) [a]	8.2	-
CCSD(T)/6-311G++(3df) [a]	6.8	-
CCSD(T)/aug-cc-pvQZ [b]	4.4	15.0
MRMP2/aug-cc-pvTZ [b]	3.3	11.5
MRCI/aug-cc-pvTZ [b]	4.6	16.3

a) Results from reference [7]
b) This work. All MRCI, MRMP2 and CCSD(T) calculations were performed at MCSCF optimized geometries

Table 2. Energy splitting between the $^2\Sigma^+$ and $^2\Pi_i$ states of AlO (kcal/mol).

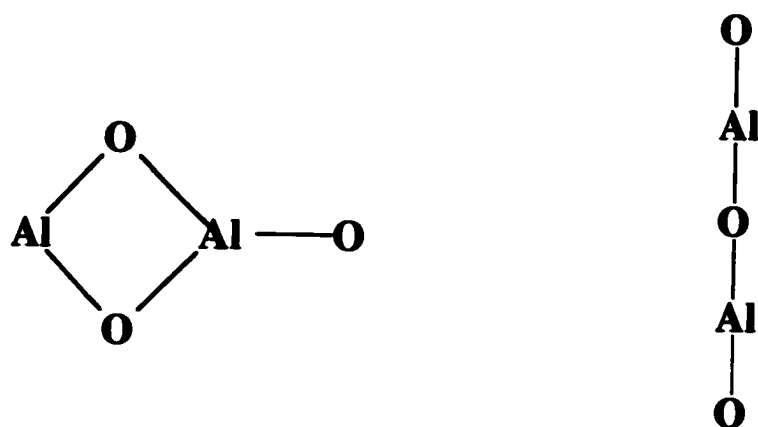| Method	$E(^2\Pi_i) - E(^2\Sigma^+)$
HF/6-311G*	-21.7
HF/aug-cc-pvQZ	-17.5
MCSCF/6-311G*	15.0
MCSCF/aug-cc-pvTZ	17.4
MCSCF/aug-cc-pvQZ	17.9
MRMP2/aug-cc-pvTZ	13.4
MRMP2/aug-cc-pvQZ	14.4
MRCI/aug-cc-pvTZ	14.4
MRCI/aug-cc-pvQZ	15.6

a)   All MRMP2 and MRCI calculations were performed at MCSCF optimized geometries
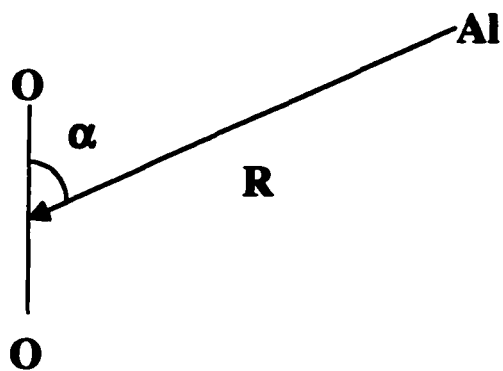
Figure 1a. Geometrical parameters of Al + O_2 reaction
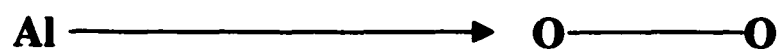
Figure 1b. Al + O_2 reaction in $C_{\infty v}$ symmetry

Figure 2. Lowest energy structures of Al_2O_3 investigated in this work

CHAPTER 7: GENERAL CONCLUSIONS

Spin-spin coupling presents a unique challenge for *ab initio* quantum chemistry, since unlike most molecular properties it is almost entirely determined (in non-relativistic theory) by the behavior of the molecular wave function in a very small region of space - around atomic nuclei. This leads to a variety of problems, including the requirements for the size of the atomic basis set and the level of electron correlation treatment. The spin-spin coupling constants are very sensitive to even the smallest changes in the electronic structure of the molecule, and since the indirect coupling is of particular significance for NMR in the liquid phase, accounting for solvent effects is also important. The theoretical part of this Dissertation addresses, at least to some extent, all of the problems mentioned above. In chapter 2, the formalism for analytic evaluation of RHF indirect spin-spin coupling constants is reviewed and various aspects of including solvent effects in the calculation of spin-spin coupling are discussed. Chapter 3 deals with the problem of suitability of Gaussian basis sets for calculations of properties related to Fermi contact interaction, as well as the electron correlation treatment requirements for such properties. It is demonstrated, although for the particularly difficult cases of boron and carbon atoms, that very large basis sets and accounting at least to some extent for excitations to all orbitals in the complete space of basis functions may be required to correctly describe spin density at the nuclei. Chapter 4 contains an original derivation of analytic hyperfine coupling tensors for MCQDPT theory. The derivation is based on the response functions formalism and incorporates some of the earlier results by other authors for analytic MCQDPT energy gradients. Once computed, the hyperfine coupling tensors can be numerically differentiated to obtain indirect spin-spin coupling constants. Future development of the

theoretical work presented in this Dissertation includes a computational study of solvation effects on RHF spin-spin coupling using the EFP model, as well as coding in GAMESS the MCQDPT hyperfine coupling tensors derived here.

The second part of this Dissertation is dedicated to the computational side of quantum chemistry. Chapter 5 deals with electronic structure of AlO_2. In chapter 6, a multi-configurational study of mechanisms of reactions of aluminum atoms with oxygen is presented. Both studies are motivated by the potential use of aluminum to improve energetic properties of solid H_2 used as a rocket fuel. Aluminum is indeed a very good candidate for the role of a HEDM additive. However, a detailed understanding of the mechanism of combustion of aluminum atoms dispersed in a solid hydrogen matrix is required to make a definitive prediction. Our results indicate that the reaction of Al with O_2 initially leads to the formation of the AlO_2 molecule. A multi-configurational analysis of the PES for AlO_2 shows that the linear form of this molecule is considerably lower in energy than the cyclic isomer. AlO_2 can dissociate to AlO and atomic oxygen without any barrier beyond the endothermicity of this reaction. There is also no barrier for the reaction of AlO_2 with AlO to form Al_2O_3, and this reaction is highly exothermic. While an additional study of the AlO_2+AlO_2 reaction is still necessary to make the final conclusion, most of our results suggest that Al_2O_3, may indeed be the main product of the Al combustion.

APPENDIX: ORIGIN OF THE δ-FUNCTION

IN THE FERMI CONTACT OPERATOR

The problem of evaluating how the momentum operator $-i\nabla$ acts on a function $f(\vec{r})$ in quantum mechanics is quite different from the problem of taking a derivative of some function $f(\vec{r})$ in standard real analysis. This difference lies in the requirement that $-i\nabla$ be a hermitean operator, i.e. for any two functions f and g

$$<f|-i\nabla|g> \ = \ <g|-i\nabla|f>^*$$ (1)

If both functions are bounded, the differentiation can be done in the usual way. However, if one of the functions has a singularity, more careful consideration may be required.

Consider an integral $\Im = \int (\vec{\nabla} r^{-3}) f(\vec{r}) d\omega$, where $f(\vec{r})$ is an arbitrary non-singular function, and the integration is done over the entire three-dimensional space. It is convenient to choose the function $f(\vec{r})$ vector-valued. Then the integral $\Im$ can be interpreted as a scalar product. For simplicity, we choose $f(\vec{r}) = \vec{r} g(r)$, where $g(r)$ is a scalar function. Since $-i\nabla$ is hermitean,

$$\Im = \int (\vec{\nabla} r^{-3}) f(\vec{r}) d\omega = -\int r^{-3} (\vec{\nabla} f(\vec{r})) d\omega = -\int r^{-3} (\vec{\nabla} \vec{r} g(\vec{r})) d\omega$$ (2)

In spherical coordinates, $\iiint dxdydz = \int_0^\infty \int_0^\pi \int_0^{2\pi} r^2 \sin\theta dr d\theta d\varphi$, and hence

$$\int r^{-3} (\vec{\nabla} \vec{r} g(\vec{r})) d\omega = -3\int r^{-3} g(\vec{r}) d\omega - \int r^{-2} g'(\vec{r}) d\omega = -12\pi \int_0^\infty r^{-1} g(r) dr - 4\pi \int_0^\infty g'(r) dr$$ (3)

Integrating the second term on the right hand side, where $g'(r) dr = d[g(r)]$,

$$-12\pi \int_0^\infty r^{-1} g(r) dr - 4\pi \int_0^\infty g'(r) dr = -12\pi \int_0^\infty r^{-1} g(r) dr - (4\pi g(r))\Big|_0^\infty$$ (4)

Using a well known property of δ-functions:

$$g(0) = \int_{-\infty}^{\infty} g(|r|)\delta(r)dr = 2\int_{0}^{\infty} g(r)\delta(r)dr \qquad (5)$$

as well as the fact that $f(\vec{r})$ is integrable and hence $f(\vec{r}) \underset{r \to \infty}{\to} 0$, obtain

$$\Im = -12\pi \int_{0}^{\infty} r^{-1}g(r)dr - (4\pi g(r))\Big|_{0}^{\infty} = -12\pi \int_{0}^{\infty} r^{-1}g(r)dr - 8\pi \int_{0}^{\infty} g(r)\delta(r)dr \qquad (6)$$

From Eq. (6) it follows that $\nabla r^{-3} = -3\vec{r}r^{-5} - 2\vec{r}r^{-4}\delta(r)$, since inserting this expression into Eq. (2) leads directly to Eq. (6). Derivatives of other singular functions can be evaluated in a similar fashion.

ACKNOWLEDGEMENTS

In addition to those whom this work is dedicated, I am greatly indebted to:

my scientific advisor, Mark Gordon - for teaching me all I know about quantum chemistry, and also for proving to me on numerous occasions that quantum chemistry is indeed a science. Mark's help was also never limited only to problems related to science or study. His kindness and care made it possible for me to survive all these years in a foreign land, and without his help this dissertation would never have been written.

Mike Schmidt - for answering so many questions about GAMESS and for very enlightening and often even entertaining discussions of various topics in theoretical chemistry.

Sergey Babionyshev - for many helpful discussion of various mathematical problems I encountered throughout my research.